

Spatiotemporal Graph Neural Networks with Uncertainty Quantification for Traffic Incident Risk Prediction

Xiaowei Gao^a, Xinke Jiang^b, Dingyi Zhuang^c, Huanfa Chen^d, Shenhao Wang^e, James Haworth^{a,*}

^a*SpaceTimeLab, University College London (UCL), London, UK*

^b*School of Computer Science, Peking University (PKU), Beijing, China*

^c*Department of Civil and Environmental Engineering, Massachusetts Institute of Technology (MIT), Cambridge, MA, USA*

^d*The Bartlett Centre for Advanced Spatial Analysis, University College London (UCL), London, UK*

^e*Department of Urban and Regional Planning, University of Florida, Gainesville, FL, USA*

Abstract

Predicting traffic incident risks at granular spatiotemporal levels is challenging. The datasets predominantly feature zero values, indicating no incidents, with sporadic high-risk values for severe incidents. Notably, a majority of current models, especially deep learning methods, focus solely on estimating risk values, overlooking the uncertainties arising from the inherently unpredictable nature of incidents. To tackle this challenge, we introduce the **S**patiotemporal **Z**ero-Inflated **T**weedie **G**raph **N**eural **N**etworks (STZITD-GNNs). Our model merges the reliability of traditional statistical models with the flexibility of graph neural networks, aiming to precisely quantify uncertainties associated with road-level traffic incident risks. This model strategically employs a compound model from the Tweedie family, as a Poisson distribution to model risk frequency and a Gamma distribution to account for incident severity. Furthermore, a zero-inflated component helps to identify the non-incident risk scenarios. As a result, the STZITD-GNNs effectively capture the dataset's skewed distribution, placing emphasis on infrequent but impactful severe incidents. Empirical tests using real-world traffic data from London, UK, demonstrate that our model excels beyond current benchmarks. The forte of STZITD-GNN resides not only in its accuracy but also in its adeptness at curtailing uncertainties, delivering robust predictions over short (7 days) and extended (14 days) timeframes.

Keywords:

Spatiotemporal Sparse Data Mining, Urban Traffic Risk Prediction, Uncertainty Quantification, Zero-Inflated Tweedie Distribution

*Corresponding author

Email addresses: xiaowei.gao.20@ucl.ac.uk (Xiaowei Gao), XinkeJiang@std.pku.edu.cn (Xinke Jiang), dingyi@mit.edu (Dingyi Zhuang), huanfa.chen@ucl.ac.uk (Huanfa Chen), shenhaowang@ufl.edu (Shenhao Wang), j.haworth@ucl.ac.uk (James Haworth)

Preprint submitted to Elsevier

September 12, 2023

1. Introduction

Urban areas, defined by their complex transportation networks and dynamic traffic patterns, are further accentuated by diverse socio-economic activities (Dai et al., 2018; Tu et al., 2020). While these features present a plethora of opportunities, they also pose significant challenges for policymakers, transportation authorities, and urban planners in managing human mobility-resulted traffic incident risks (Barahimi et al., 2021; Rodrigue, 2020). Such risks negatively impact urban sustainability, leading to human casualties, economic losses, and diminished livability. Addressing these concerns necessitates the development of predictive models that can effectively identify high-risk zones and reliably anticipate potential incidents (Laureshyn et al., 2017; Zhou et al., 2021).

Traffic incident prediction is an interdisciplinary domain, intersecting urban planning, transportation engineering, data science, and social sciences (Zhou et al., 2020; Yu et al., 2020b; Bibri, 2018). The overarching aim is to discern patterns from historical spatiotemporal incident risk data to profile or forecast traffic incidents (Chakraborty et al., 2019; Liu et al., 2022). The current literature in this realm can be classified into two predominant categories:

- *Incident injury severity identification and analysis*: Researchers focus on extracting patterns, causes, and contributing factors related to injury severity from historical incident data. The objective is to understand the interplay between various determinants such as road attributes, traffic conditions, weather conditions, and human behaviour, and their impact on individual injury severity levels (Hu et al., 2010; Benlagha and Charfeddine, 2020; Ma et al., 2021; Yang et al., 2021, 2022).
- *Incident risk prediction by spatiotemporal modelling*: Given the significance of spatiotemporal attributes, researchers have increasingly emphasized modelling the dynamics and exposures in urban environments related to incident risk. This involves capturing the spatial dependencies among different road segments and considering the temporal variations in traffic patterns (Wang et al., 2022a). By incorporating spatiotemporal modelling techniques, researchers can effectively account for the evolving nature of urban traffic and improve the accuracy of incident risk predictions.

Both methodologies offer advantages yet bear intrinsic constraints. As Liu et al. (2023) underscores, injury severity causal analysis may not reliably forecast future incidents. On the flip side, spatiotemporal modelling, while presenting a comprehensive approach with the potential for enhanced accuracy, faces challenges regarding imbalanced incident data and unreliable results.

Delving deeper into traffic incident risk prediction research, these challenges can be elaborated upon as follows. The first is summarized as the **zero-inflation issue**, a characteristic of risk data at fine-grained levels (Trirat et al., 2023; Zhou et al., 2020). The issue describes the excessive quantity of zeroes due to data sparsity. Conventional modelling approaches often dilute this issue by aggregating risk values at more extensive regional scales (Bao et al., 2019; Wang et al., 2021c). While this might yield reasonable predictions from both broader and smaller regional perspectives, it leads to unsatisfactory estimates at road levels plagued by overdispersion. Hence, there is a pressing need for innovative modelling techniques capable of accurately capturing and representing zero-inflation patterns in traffic incident risk data.

A second pressing issue pertains to **uncertainty quantification (UQ)**. Broadly, uncertainty can be divided into epistemic and aleatoric types, signifying model and data uncertainty, respectively (Qian et al., 2022). Due to their unpredictable and sporadic nature, traffic incidents serve as typical examples of aleatoric uncertainty, which is irreducible compared to the epistemic one (Bao et al., 2019; Zhou et al., 2021). While current deep learning models excel at learning intricate patterns and accurately predicting the *average risk*, they often implicitly

assume homoskedasticity (uniform variance) and then inadequately account for the inherent variability in the results of their predictions (Wang et al., 2023a; Zhuang et al., 2022; Jiang et al., 2023). Additionally, while some strides have been made in UQ for time-series data prediction (Wu et al., 2023; Zhu et al., 2022; Li et al., 2022c), such efforts are still scarce in sparse data, particularly in risk prediction.

To address the aforementioned challenges, our approach prioritizes UQ, with a specific focus on the prediction interval of risk estimation. We introduce a novel approach — the Spatiotemporal Zero-Inflated Tweedie Graph Neural Network (STZITD-GNNs)— for the finest granularity at the road level among existing spatiotemporal deep learning models that consider UQ. This method is designed to boost the proficiency of spatiotemporal deep learning models in UQ by interacting with the statistical methods, consequently improving the robustness of road-level risk prediction.

Our concentrated focus on finer spatiotemporal granularity naturally results in a more substantial graph structure compared to traditional grid-based datasets. This poses considerable challenges in efficiently handling node embeddings and producing outputs. Furthermore, road segments typically present a low degree of observed daily risk, with a large majority displaying no incidents occurrence throughout the year. This results in an extremely unbalanced dataset, exhibiting significant zero-inflation for risk assessment (Zhou et al., 2020; Wu et al., 2022). Meanwhile, the distribution of risk severities’ frequency also follows a skewed and long-tailed pattern. The majority of incidents are categorized as minor in severity, contributing to slight risk (Shirazi and Lord, 2019; Saha et al., 2020). Given these circumstances, the common assumption of a Gaussian distribution for entities in graph neural network prediction becomes unsuitable (Wang et al., 2023a). While the state-of-the-art approach proposed by Zhuang et al. (2022) provides encouraging results for UQ in sparse travel demand scenarios, their methodology—grounded in the negative binomial (NB) distribution—limits its focus to binary outputs, neglecting the real full distribution of incident risk values in our problems.

To further overcome the above limitations, we propose the use of the Tweedie (TD) distribution, a compound Poisson-gamma distribution, which simultaneously models the exact zero values and the continuous positive values. The TD model’s variance function is analogous to that in the NB model but incorporates a flexible index parameter $\rho \in (1, 2)$ (Lord and Mannering, 2010; Shirazi and Lord, 2019). The TD distribution has been extensively used in various domains with overdispersion data, including crash frequency estimation (Wang et al., 2019), insurance claims (Smyth and Jørgensen, 2002), actuarial studies (Shi (2016)), and meteorological precipitation (Dunn, 2004).

However, when confronted with the challenge of extremely unbalanced zero-inflated data and skewed positive data in urban risk values, the TD distribution alone may not provide satisfactory performance as it cannot capture both aspects of the distribution (Khosravi et al., 2010; Abe and Yadohisa, 2017)). Therefore, we propose a mixture model strategy known as the "Zero-Inflated Tweedie" (ZITD) model. Unlike the traditional TD model, the ZITD model incorporates an additional parameter π to estimate the probability mass of zero values, in addition to the parameters of the TD model component. This allows for a more comprehensive understanding of risk values, accounting for both the zero mass and the skewed positive component of the distribution.

Unlike conventional methodologies that estimate spatial and temporal outputs separately before fusing them (Zhuang et al., 2022; Wang et al., 2023a), our approach harnesses the power of joint spatiotemporal graph neural networks to simultaneously estimate and fit the four parameters of the ZITD probabilistic distributions. In detail, we employ a Gated Recurrent Unit (GRU) as the temporal encoder and a Graph Attention Network (GAT) as the spatial encoder. These components work in tandem to simultaneously capture the intricate spatiotemporal dependencies in the data. Through extensive empirical evaluation using real data from three boroughs of London, UK, we provide compelling evidence of the superior performance of our model in road-level urban risk prediction tasks. Our major contributions can be summarized as follows:

- We propose a novel framework, STZITD-GNNs, for estimating the spatiotemporal uncertainty of traffic incident risk, specifically addressing the challenges posed by extremely unbalanced zero-inflated and long-tail data at the road level. By incorporating probabilistic GNNs, our framework successfully quantifies the sparse and discrete uncertainty, particularly in high-resolution risk datasets.
- Through the integration of spatiotemporal graph neural networks (ST-GNNs), our framework jointly captures the temporal dynamics and spatial relationships within urban data, enabling a holistic insight into the inherent uncertainties and intricate risk patterns and also ensuring a robust and nuanced approach to urban risk assessment.
- Extensive experiments are conducted on real-world datasets to evaluate the performance of the STZITD-GNNs. The results demonstrate that our proposed method surpasses state-of-the-art methods, validating the effectiveness and superiority of the STZITD-GNNs framework in tackling sparse urban risk prediction challenges.

To our knowledge, our research advances traffic incident risk prediction by transitioning from deterministic deep learning to a probabilistic approach, emphasizing road-level over grid-based models. This method adeptly tackles the zero-inflation and long-tail distribution in granular risk data, enhancing accuracy in traffic incident risk assessment. Our study underscores the importance of UQ in road-level risk prediction, providing pivotal insights for future research and applications.

This manuscript is structured as follows: In Section 2, we conduct a rigorous review of spatiotemporal modelling methodologies in the domain of traffic risk prediction and then delve into Uncertainty Quantification (UQ). Section 3 provides a detailed description of the proposed model. Section 4 compares our empirical results against state-of-the-art benchmark models, further augmenting our assertions with illustrative visualizations. In Section 5, we delineate the salient attributes of our model and suggest avenues for future enhancements.

2. Literature Review

2.1. Traffic Incident Risk Prediction under Spatiotemporal Modelling

Traffic incident risk prediction is a crucial aspect of urban planning and mobility management. Early studies in this field have primarily relied on traditional statistical methods or classical machine learning techniques to analyze and forecast incidents on specific road segments or highways. These approaches include regression models (Caliendo et al., 2007; Bergel-Hayat et al., 2013), Bayesian Networks (Hossain and Muromachi, 2012), tree-based models (Chong et al., 2004; Lin et al., 2015), and k-nearest neighbour method (Lv et al., 2009). However, these studies have initially focused on small areas, limiting their applicability to broader risk management knowledge and considering only a limited set of influential factors.

Recognizing the need to overcome these limitations, researchers have expanded their investigations to encompass broader traffic zones, such as borough or citywide levels, to provide a more comprehensive understanding of urban risk (Chang and Chen, 2005; Anderson, 2009; Zhang et al., 2014). However, it is crucial to acknowledge that risk data possess inherent complexities in their spatial and temporal attributes, which pose challenges that these classical approaches may not effectively address. These methods often handle the individual incident data separately without considering the interdependencies among different locations, which can result in inadequate accuracy levels in risk prediction (Wang et al., 2021a). Moreover, when dealing with larger areas characterized by finer spatial units, the limitations of these traditional methods become more pronounced.

To overcome these challenges, recent advancements in deep learning techniques have shown promise in urban traffic risk prediction by leveraging the power of spatiotemporal modelling. Convolutional Neural Networks (CNNs), Recurrent Neural Networks (RNNs), and Graph-based networks, like Graph Convolution Networks (GCNs), have demonstrated their effectiveness in capturing intricate spatial patterns, capturing temporal dependencies, and modelling complex interactions among urban areas (Wang and Cao, 2021; Liu et al., 2020). As summarized in Table 1, Chen et al. (2016) were among the first to explore national-wide risk prediction by employing a Stack Denoise Autoencoder. They integrated human mobility GPS data and historical incident point data at the grid level to map the real-time risk situation in Tokyo. However, while their approach attempted to capture a larger spatial area, it did not consider geographical content for precise and long-term risk prediction. Later, Chen et al. (2018) introduced a Stack Denoise Convolutional Autoencoder that incorporated spatial dependencies in incidents using stacked CNNs. Nonetheless, both of these studies overlooked the influence of temporal factors. Although RNNs are capable of handling temporal information, they are more suited for short-term temporal learning (Ren et al., 2018). To better address the temporal aspect, Ren et al. (2018) utilized multiple Long Short-Term Memory (LSTM) to consider temporal influential factors among several spatial locations and predict risk at the city level. Their work represented the first attempt to incorporate temporal factors in deep learning models for city-wide traffic risk prediction. Similarly, Moosavi et al. (2019) employed LSTM networks for national-wide risk prediction, demonstrating their efficacy in predicting risk at 15-minute intervals. Building upon the LSTM framework, Yuan et al. (2018) proposed a more advanced model known as the Convolutional Long Short-Term Memory (Hetero-ConvLSTM) neural network based on heterogeneous data. This model aimed to jointly address spatial heterogeneity and capture temporal features in state-wide incident prediction. However, their approach relied on pre-defined moving windows based on the spatial features of Iowa, United States, limiting its generalizability to other cities. Bao et al. (2019) integrated CNNs, LSTM as well as ConvLSTM into a spatiotemporal convolutional long short-term memory network (STCL-Net). Their work presented a more practical and feasible approach for city-wide traffic risk prediction. By combining the strengths of these models, the STCL-Net effectively captured the spatiotemporal dependencies in the risk data and influential factors, leading to improved prediction performance.

Furthermore, in order to capture both local and global dynamics with hierarchical spatial information, Zhu et al. (2019) proposed the Deep Spatiotemporal Attention Learning Framework. Unlike previous approaches that primarily focused on local risk information, this framework incorporated a spatiotemporal attention mechanism to effectively capture the dynamic impact of traffic risk at different levels. One notable aspect of their work was the emphasis on using real traffic administrative areas instead of manually divided grids. This approach enabled more realistic modelling of spatial heterogeneities in traffic incidents, thereby reducing prediction deviations and enhancing the accuracy of risk prediction. In a similar vein, Huang et al. (2019) proposed the deep Dynamic Fusion Network (DFN) framework, which dynamically aggregated heterogeneous external factors. This framework allows for the effective fusion of diverse data sources, enabling a comprehensive understanding of the spatiotemporal dynamics of risk factors.

The utilization of Graph-based networks has emerged as a prominent approach in addressing city-wide traffic risk prediction tasks by leveraging the spatial graph features inherent in urban networks or regions. This approach takes advantage of the spatial graph features derived from real urban elements, enabling more effective modelling and prediction of traffic risk throughout a city (Xue et al., 2022; Cheng et al., 2022; Li et al., 2022a,b).

For instance, Zhou et al. (2020) constructed an urban graph based on urban regions and proposed the RiskOracle framework, which integrates the Differential Time-varying Graph Neural Network (DTGN). They learned dynamic subregion-wise correlations between historical traffic status and traffic risk, achieving joint prediction for traffic flow and risk. Notably, to address the zero-inflation issue in the risk data, they employed an a priori knowledge-based data enhancement (PKDE) strategy to define the subregional risk labels during the training process. This strategy utilized two experiencing parameters to transform zero risk values within

the range of 0 and 1 while preserving the order of the real risk situation. Building upon this work, Zhou et al. (2022b) enhanced the DTGN framework by incorporating an LSTM-based hierarchical sequence learning structure. This enhancement considered multi-scale historical spatiotemporal information for both long-term and short-term predictions.

In a similar vein, Wang et al. (2021a) devised three distinct graph structures: risk, road, and Points of Interest (POI), to capture the semantic relationships among regions in their graph. They proposed two modules for risk forecasting: a Spatiotemporal Geographical Module that captured the geographical spatiotemporal correlations, and a spatiotemporal Semantic Module that described the semantic spatiotemporal correlations based on the three similarity graph structures. To address the zero-inflation issue, they introduced a weighted loss function that focused on the non-zero risk values, thereby mitigating the risk of overfitting. However, it is important to note that this work primarily focuses on static geographic semantic similarities and is not capable to deal with graph unaligned problems. In a similar vein, Wang et al. (2021b) proposed a Multi-View Multi-Task Spatio-Temporal Networks model for jointly predicting fine- and coarse-regional traffic incident risks. Their approach integrated attention-based LSTM, channel-wise CNN, and multi-view GCN along with multiple loss functions to facilitate multi-view prediction and contain a mutual constraint for the finer-level loss. While their work considered the zero-inflation issues in a cross-level corresponding prediction task, it may not be an optimal solution when the primary focus is on fine-level risk prediction. In contrast, Trirat et al. (2023) proposed a multi-view graph neural networks framework with a multi-attention module to incorporate dynamic similarity information from traffic status and also static geographic semantic similarities. By integrating this dynamic information, their approach provides a more comprehensive understanding of dangerous driving behaviour and traffic incidents and enables a more accurate prediction of urban traffic risk. The Huber loss function serves as a compromise between squared error and absolute error losses, allowing for a robust regression process that avoids being overly influenced by many zero values.

Recently, there have been a few works attempting to utilize graph-based deep learning methods to address road-level risk prediction tasks. Yu et al. (2021) conducted road-level risk prediction using a novel Deep Spatiotemporal Graph Convolutional Network. They defined three network layers, treating the road graph as an independent layer, and incorporating heterogeneous spatiotemporal data in the second Spatiotemporal Convolution Layer and an Embedding Layer. To address the zero-inflation issue, they employed an Undersampling method, which balanced the number of risky road samples and non-risk road samples and treated incident risk as a binary classification task. Although their approach demonstrated promising results at the road-level granularity, the output only indicates the presence or absence of incidents, thus masking the true risk situation of individual roads with limited sample information. Wu et al. (2022) proposed a fully connected and dynamic network framework for predicting road-level risk by capturing dynamic spatiotemporal correlations. They addressed the zero-inflation issues by incorporating a cost-sensitive learning module, which improved the classification accuracy of positive samples without compromising the overall accuracy. This module considered a probability fault cost based on the ratio of zero to non-zero values, allowing for more constraints on non-zero risk value outputs.

2.2. Uncertainty Quantification (UQ) in Spatiotemporal Prediction

With an increasing focus on solving a multitude of spatiotemporal prediction problems, UQ has found broad applications in areas ranging from air pollution (Wu et al., 2021) and traffic demand (Wang et al., 2023a; Zhuang et al., 2022) to traffic speed (Wu and James, 2021), epidemic transitions (Lin et al., 2021), and climate change (Thornton et al., 2021), among others. Current UQ methods are generally bifurcated into two schools of thought: the Bayesian and Frequentist perspectives.

In the Bayesian framework, the aim is centred around parameter inference, grounded in Bayes' theorem.

Table 1: Summary of Deep Learning Methods in Spatiotemporal Prediction

Reference	Methodology	Spatial Unit	Zero-Inflate Issue
Chen et al. (2016)	Stack Denoise Autoencoder	0.5km*0.5km Grid	/
Ren et al. (2018)	Long Short-term Memory network	1km * 1km Grid	/
Chen et al. (2018)	Stack Denoise Convolutional Autoencoder	Grid	/
Yuan et al. (2018)	Convolutional Long Short-Term Memory	5km * 5km Grid	/
Moosavi et al. (2019)	Long Short-term Memory Network	5km * 5km Grid	/
Zhu et al. (2019)	Deep Spatial-Temporal Attention Learning Framework	Urban administrative areas	/
Huang et al. (2019)	Dynamic Fusion Network	Grid	/
Bao et al. (2019)	Spatiotemporal Convolutional Long Short-term Memory Network	8 * 3 Matrix Cells 15 * 5 Matrix Cells 30 * 10 Matrix Cells	/
Zhou et al. (2020)	Differential Timevarying Graph Neural Network	1.5km*1.5km Grid	A priori knowledge-based data enhancement strategy
Wang et al. (2021a)	Geographical and Semantic Spatiotemporal Network	2km * 2km Grid	Weighted Loss Function
Wang et al. (2021b)	Multi-View Multi-Task Spatio-Temporal Networks	20*20 Matrix Cells	Cross-view mutual beneficial prediction
Yu et al. (2021)	Deep Spatio-Temporal Graph Convolutional Network	Road Segment	Undersampling method
Wu et al. (2022)	Multi-attention Dynamic Graph Convolution Network	Road Segment	Cost-sensitive Learning Loss Function
Zhou et al. (2022b)	Differential Timevarying Graph Neural Network	1.5km*1.5km Grid	A priori knowledge-based data enhancement strategy
Trirat et al. (2023)	Multi-view Graph Neural Networks Framework with a Multi-attention Module	Urban administrative areas	Huber Loss Function

This approach models the posterior distribution of the network parameters, $p(\theta|x, y)$, for a given input-target pair, (x, y) , predicated on the assumption of a known prior probability distribution over these parameters, $p(\theta)$ (Gawlikowski et al., 2021). According to comprehensive surveys by Gawlikowski et al. (2021) and He and Jiang (2023), primary methods for inferring the posterior distribution are threefold: Laplace approximation based on the second derivative of likelihood, Markov Chain Monte Carlo (MCMC) -based Sampling methods, and Variational Inference (VI) predicated on a parametric distribution. Each of these methods has found application in addressing Spatiotemporal Traffic-related UQ problems. For instance, Qian et al. (2022) employed a Gaussian distribution to encapsulate the aleatoric uncertainty, while combining VI and MC sampling to estimate the epistemic uncertainty in the 5-minute traffic flow prediction on an hourly basis. Kong et al. (2023) and Wu and James (2021) incorporated VI into GNN to quantify traffic condition uncertainty, specifically concerning speed and flow. However, they mainly considered temporal information due to computational complexity constraints. In contrast, Wu et al. (2021) utilized the MCMC-based method to quantify uncertainty in limited node-restricted forecasting tasks regarding air pollution, sensor-based traffic flow, and state-based COVID death prediction. Liu et al. (2022) designed Bayes by Backpropagation and local reparameterization techniques to capture the weight distribution of models, thus achieving freeway incident detection. Nevertheless, their method only provided short-term predictions of up to 30 minutes, owing to the disregard of spatial features. To summarize, the primary challenge associated with the Bayesian approach lies in its computationally intensive processing step, which poses significant scaling challenges for finer-level spatiotemporal forecasting (Wang et al., 2023a; Zhuang et al., 2022; He and Jiang, 2023). Moreover, the common approximation process shared among the discussed Bayesian works contributes to an irreducible inaccuracy in UQ (Gawlikowski et al., 2021; Wang and Yeung, 2020).

In stark contrast to the Bayesian approach, the Frequentist perspective primarily relies on Mean-Variance Estimation (MVE), enjoying the advantages of computational efficiency and flexible model structure tuning with fewer prior-knowledge constraints (Wu et al., 2023). Traditional models that produce single-point outputs are supplanted by MVE’s ability to furnish a predictive distribution. In this framework, it is postulated that the outputs are consistent with a specific parameterized family of probability distributions, typically falling within the Gaussian distribution (Chen et al., 2020; Wang et al., 2023a). Therefore, MVE’s objective is the minimization of the loss function associated with the parameters anticipated by the model. Consequently, this technique provides a detailed representation of potential outcomes, encouraging a deeper understanding of inherent uncertainties within the predictions.

Two primary methods can be discerned within this perspective: parametric and non-parametric. Parametric methods predict values based on the parameterized distributions derived from the parameters of the neural networks (Wang et al., 2023a; Khosravi and Nahavandi, 2014). In contrast, non-parametric methods concentrate on establishing the upper and lower bounds or employ quantile regression to obtain the prediction intervals (PIs) (Pearce et al., 2018; Khosravi et al., 2010; Koenker and Hallock, 2001; He and Jiang, 2023; Gawlikowski et al., 2021).

For instance, both Guo et al. (2014) and Lin et al. (2018) applied non-parametric methods to ascertain the upper and lower bounds of short-term traffic flow predictions. Guo et al. (2014) employed an adaptive Kalman filter to dynamically map volatile traffic flow, thus achieving real-time UQ. Lin et al. (2018) combined Particle Swarm Optimization (PSO) with the Extreme Learning Machine (ELM) neural network to predict PIs, leading to a more precise individual assessment of upper and lower bounds. In a different approach, Li et al. (2022c) adapted the traditional ConvLSTM model, integrating it with a differentiable PI-oriented loss function to attain long-term highway traffic flow predictions and UQ encapsulation. Nevertheless, these works, primarily concerned with traffic flow prediction, tend to approach UQ from a temporal series perspective, neglecting spatial UQ. Moreover, Zhou et al. (2021) introduced a novel spatiotemporal UQ framework that accounted for differences in regional traffic situations and a hierarchical data turbulence scheme. They utilized an out-of-

distribution noise parameter to encapsulate the predicted PIs. Despite promising results, their model depends on dense data input. While non-parametric methods are not as restricted by prior data knowledge, they are heavily reliant on abundant data input and advanced method structures, which reduces their applicability in complex urban environments.

On the other hand, parametric methodologies typically introduce auxiliary probabilistic layers to seize pertinent parameters, thus achieving minimal alterations to the existing training structures. UQ is calculated in this approach via parameter-driven intervals, in tandem with mean values and variance. Wang et al. (2023a) offered a thorough examination of diverse Gaussian-based probabilistic suppositions incorporated with GNNs, thereby formulating a generalized framework for quantifying spatiotemporal uncertainty in travel demand. They proposed that the adoption of suitable probabilistic suppositions is pivotal for achieving stable UQ while exerting minimal impact on single-point estimation. As noted by Wang et al. (2023a), these strategies are heavily dependent on predefined data distributions. While parametric methodologies for UQ present computational efficiency and facile adaptability, exploration concerning sparse and event-centric traffic data remains conspicuously scarce. The most recent pioneering work in this field is Zhuang et al. (2022), who were among the first to address the issue of sparse data in the context of UQ. Instead of using the Gaussian assumption, they introduced a three-parameter zero-inflated negative binomial distribution combined with spatiotemporal neural networks to simultaneously manage the predominant zero instances and non-normal distribution in sparse travel demand data. Despite the commendable merits of their innovative method and impressive results, they encountered practical challenges when zero values were overly extreme and in non-time series traffic scenarios, particularly in event-based traffic risk situations.

3. Methodology

In this section, we start by introducing the important concepts and defining the framework for the real-world problem of road-level traffic risk prediction under study in Section 3.1. We then illustrate the progression from the TD distribution to ZITD within the context of UQ in Section 3.2. Subsequently, we introduce our novel STZITD-GNNs model, a spatiotemporal probabilistic modelling framework designed for ZITD-based UQ, that combines the strengths of the GRU and GAT in Section 3.3. The section finishes with an in-depth exploration of the loss function employed within our model in Section 3.4. The major notations used in this section are listed in Table 2.

3.1. Preliminaries and Problem Definition

This section lays out the foundational concepts and terminology pertinent to the study, followed by a precise statement of the problem at hand.

Definition 1. Road Traffic Incident Risk: A traffic incident refers to an incident involving one or more road users, leading to physical injury, loss of life, or damage to property. We denote the set of roads as V of size $N = |V|$, where v_i signifies the i^{th} road. Traffic risk on roads is represented as $Y \in \mathbb{R}^{N \times T}$ for a duration of T minutes, and y_{it} denotes the traffic risk at the t^{th} time slot for road v_i . Thus, $Y_t \in \mathbb{N}^N$ signifies the traffic risk for all roads at the t^{th} time slot, where y_{it} is its constituent element. The computation of traffic risk y_{it} for road v_i at time slot t is given by:

$$y_{it} = \sum_{j=1}^{C_{it}} l_{it}^{(j)}, \quad (1)$$

Table 2: Main notations in this paper

Notation	Description
Y / X	Road-level traffic risk / Road-level spatiotemporal traffic feature
$V / E / A$	Road set / Edge set / Road adjacency matrix
$v_i / (v_i, v_j)$	The i^{th} road / Edge between the i^{th} road and the j^{th} .
N / T	Numbers of roads / Time length
C_{it}	Number of incidents on road v_i at time slot t
l_{it}^j	The j^{th} cardinality values of incident severities at time slot t for road v_i
$d / F / F'$	Feature dimension/Temporal feature dimension/Spatio-Temporal feature dimension
\mathcal{ST}	Spatiotemporal deep learning Model
$f_{TD}(\cdot)$	Probabilistic density function of Tweedie Distribution
$\rho / \phi / \mu / \pi$	Index parameter/ Dispersion parameter/ Mean parameter/ Zero-inflated parameter
$\theta / \lambda / \alpha, \gamma$	Natural parameter / Poisson mean parameter / Gamma parameters
$\mathcal{Z}_T / \mathcal{Z}$	Temporal embedding / Spatiotemporal embedding
$\text{ReLU}(\cdot) / \sigma(\cdot) / \text{LeakyReLU}(\cdot) / [\cdot]$	ReLU activation / Sigmoid activation / LeakyReLU activation / Concatenation
$W_r, W_u, W_c, W_a, b_r, b_u, b_c, \vec{a}$	Learnable weight matrices of GRU and GAT
$W_\pi, W_\mu, W_\phi, W_\rho, b_\pi, b_\mu, b_\phi, b_\rho$	Learnable weight matrices of the four Parameter Encoders
$h_t / r_t / u_t$	Hidden feature / Reset gate / Update gate
$\alpha_{i,j}$	Attention value between road v_i and v_j
M	Number of attention heads
ϵ	The minimum value
η	L2 normalization weight-parameter

where C_{it} denotes the number of incidents, and $l_{it}^{(j)}$ represents the j^{th} severity level of incidents at time slot t for road v_i . We allocate the incident point to its closest road. As per prior research (Wang et al., 2021a; Trirat et al., 2023), l is assigned the values 1, 2, and 3, representing minor, injury, and fatal incident severities, respectively. y_{it} equals 0 if there are no traffic incidents, i.e., $C_{it} = 0$.

Definition 2. Spatiotemporal Features: Road features are represented as $X \in \mathbb{R}^{N \times T \times d}$, where d is the dimension of the spatiotemporal road features. We denote x_{it} as the spatiotemporal feature of road v_i at the t^{th} time slot. Accordingly, $X_t \in \mathbb{R}^{N \times d}$ signifies the spatiotemporal feature of all roads at time slot t . Our study includes spatial features like geographical information, general road conditions, and census features. Temporal features, which vary daily, encompass weather information such as sunrise and sunset times, humidity, visibility, rainfall, etc., along with the designation of the day as a holiday or a working day.

Definition 3. Road Connection Graph: Keeping the connectivity of roads in mind, we construct the road network graph $\mathcal{G} = (V, E, A)$. Here, E denotes the edge set, and $A \in \mathbb{R}^{N \times N}$ is the adjacency matrix that describes the connections between roads. An entry $A_{i,j} = 1$ indicates the existence of an edge between road v_i and v_j , denoted as $(v_i, v_j) \in E$, while $A_{i,j} = 0$ implies no connection, denoted as $(v_i, v_j) \notin E$.

In line with Tobler’s First Law of Geography (Tobler, 1970), spatial correlation bears a significant relationship with geographic distance (Yu et al., 2020a; Zhou et al., 2021; Wang et al., 2023b). This implies that the geographical proximity between two roads directly influences the correlation of traffic risk effects: the closer the roads, the stronger the correlation. As a result, traffic incidents often lead to spatial spillover effects, suggesting that a risk point on one road can have a significant impact on its neighbouring roads. To encapsulate this spatial attribute, we employ random walks (Perozzi et al., 2014; Li et al., 2017; Hamilton, 2020) as a simulation process. In this procedure, we use the adjacency matrix A to disperse road traffic risks to their closest neighbours, adhering to three predefined thresholds: a diffusion probability, a road-level traffic risk reduction factor, and a maximum hop count.

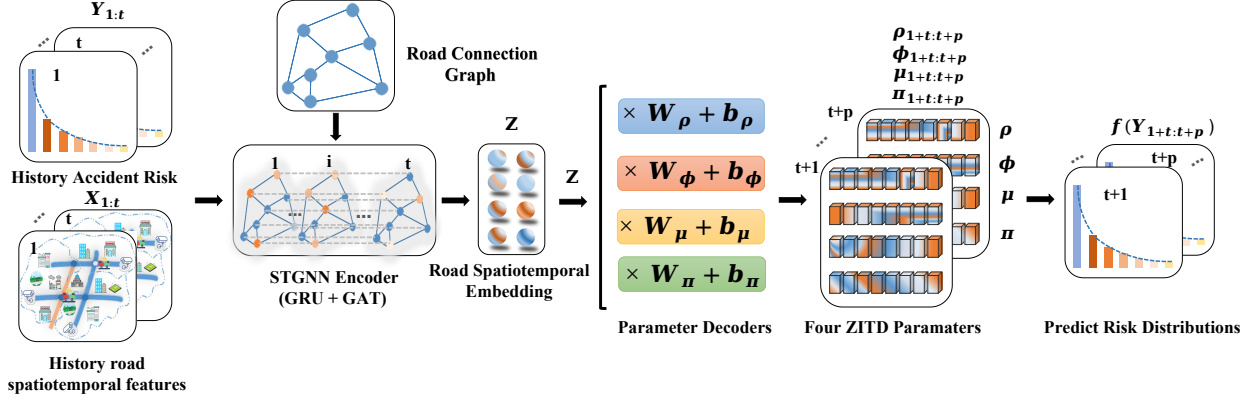


Figure 1: The overall framework of STZITD-GNNs. STZITD-GNNs utilize ST-GNN Encoder \mathcal{ST} (composed by GRU and GAT encoders) to encode the history time window $1:t$ incident risk $Y_{1:t}$ and road spatiotemporal features $X_{1:t}$ with use of road connection graph into road spatiotemporal embedding \mathcal{Z} at first. After encoding, the four parameter decoders map \mathcal{Z} into ZITD parameter space and obtain $\pi_{t+1:t+p}, \mu_{t+1:t+p}, \phi_{t+1:t+p}, \rho_{t+1:t+p}$ for predicted time window $t+1:t+p$, which determine the predict feature road traffic risk distribution $f(Y_{t+1:t+p})$.

Problem Definition: The aim of our model is to predict the future expected traffic incident risk and the confidence interval of predicted results per road, with a forecast horizon of p time windows, based on N roads and their traffic risk across time windows of length T minutes. Essentially, this is a sequence-to-sequence prediction task. The objective is to utilize historical records $X_{1:t}, Y_{1:t}$ and the graph structure A as input data for training, to predict the probabilistic density function $f(Y_{t+1:t+p})$ of the distribution of $Y_{t+1:t+p}$ (i.e., the traffic risk distribution for the next p time windows). This facilitates the analysis of future road-level traffic risk expectations and confidence intervals:

$$\mathcal{ST}_{\Theta}([X_{1:t}, Y_{1:t}], A) \rightarrow f(Y_{t+1:t+p}), \quad (2)$$

where Θ denotes the learned parameters for the ST-GNN model (also referred to as \mathcal{ST}). The predictions are made for both a 14-day input to a 14-day output and a 7-day input to a 7-day output.

3.2. From TD Distribution to ZITD Distribution

This subsection provides an in-depth exploration of the progression from TD to ZITD distribution in the specific context of road risk prediction. Building on the work of Lord and Mannering (2010) and Smyth and Jørgensen (2002), we recognize the effectiveness of TD distribution in addressing over-dispersed data, indicating its potential applicability in road-level traffic risk prediction.

As illustrated in Section 3.1, when we aggregate risk data (incorporating various severities of crashes) from different road segments or identical segments over different time intervals, the resulting distribution of risk counts tends to exhibit over-dispersion of varying degrees. In these scenarios, the variance of risk counts outstrips the mean risk count, creating a deviation from the Gaussian distribution, as underlined by the work of Halder et al. (2019) and Wang et al. (2023a).

In detail, a defining feature of overdispersed risk data—applying to both incident counts and the associated severity—is the prevalence of ‘excess’ zeros, implying more zero entries than would be predicted under a corresponding Poisson process. Conversely, we observe a skewness in non-zero outcomes, specifically a left-skewed

distribution representing a smaller proportion of higher risk values. This unique pattern, combined with the long-tail distribution of risk data, necessitates a robust modelling approach. In transitioning from the TD to the ZITD distribution, our model accommodates these intrinsic traits of overdispersed and long-tail data. It not only addresses the issue of excess zero counts innovatively but also accurately captures the left-skewness of non-zero outcomes, making it a more fitting tool for road-level traffic risk prediction.

3.2.1. TD Distribution

In adherence to Equation 1, we designate y_k as the risk value of road i on day t . As a special case of Exponential Dispersion Models (EDMs), the TD model encompasses a broad family of statistical distributions (Tweedie et al., 1984; Jørgensen, 1987; Jiang et al., 2023). A random variable following the TD distribution possesses a probability density function, f_{TD} , with its probability density function computed as follows (Jørgensen, 1987):

$$f_{TD}(y_k|\theta, \phi) \equiv a(y_k, \phi) \exp \left[\frac{y_k(\theta) - \kappa(\theta)}{\phi} \right], \quad (3)$$

here, $\theta \in \mathbb{R}$ represents the natural parameter, while $\phi \in \mathbb{R}^+$ stands for the dispersion parameter. The normalizing functions $a(\cdot)$ and $\kappa(\cdot)$ are parameter functions for ϕ and θ , respectively, detailed further in the subsequent discussion. For a TD distribution of EDMs, the mean and variance of variable y_k are given by:

$$E(y_k) = \mu = \kappa(\theta)', \quad Var(y_k) = \phi \kappa(\theta)'', \quad (4)$$

In these equations, $\kappa(\theta)'$ and $\kappa(\theta)''$ represent the first and second derivatives of $\kappa(\theta)$, respectively. Meanwhile, $\mu \geq 0$ functions work as the mean parameter. Since the mean $E(y_k)$ and variance $Var(y_k)$ are dependent, $\kappa(\theta)''$ can be directly expressed as $V(\mu)$, thereby providing a direct mean-variance relationship (Mallick et al., 2022). Additionally, the TD family encompasses a number of vital distributions for distinct index parameters ρ as demonstrated by $V(\mu) = \mu^\rho$. These include the Normal ($\rho = 0$), Poisson ($\rho = 1$), Gamma ($\rho = 2$), Inverse Gaussian ($\rho = 3$), and Compound Poisson-Gamma distribution ($1 < \rho < 2$) and could be refer to Appendix A. The Compound Poisson-Gamma distribution is particularly applicable, given its practical prowess in parameterizing zero-inflated and long-tailed data, which aligns with the observed characteristics of real traffic risk data scenarios.

The frequency of traffic risk C_k adheres to a Poisson distribution represented by $Pois(\lambda)$ with a mean of λ , expressed as $C_k \sim Pois(\lambda)$. This is natural as the frequency often appears as the main prediction target in the previous literature (Zhou et al., 2020; Trirat et al., 2023). Concurrently, the incident severity $l_k^{(j)}$ are modelled as independent and identically distributed *i.i.d* Gamma random variables, $C_k \perp l_k^{(j)}$ and $\forall j$, denoted as $Gamma(\alpha, \gamma)$. These variables bear a mean of $\alpha\gamma$ and a variance of $\alpha\gamma^2$, as $l_k^{(j)} \stackrel{iid}{\sim} Gamma(\alpha, \gamma)$. C_k and $l_k^{(j)}$ together form the modelling of the occurrence of a single incident. Consequently, the traffic incident risk y_k is formulated as a Poisson sum of these iid Gamma random variables. Corresponding to Equation 1 and considering $1 < \rho < 2$, we can finally reformulate the random variable y_k as follows:

$$y_k = \begin{cases} 0 & \text{if } C_k = 0, \\ \sum_{j=1}^{C_k} l_k^{(j)} = l_k^{(1)} + l_k^{(2)} + \dots + l_k^{(C_k)} & \text{if } C_k > 0. \end{cases} \quad (5)$$

In the scenario where $C_k = 0$, we correspondingly have $y_k = 0$. The probability density at zero for traffic incident risk, therefore, becomes $\mathbb{P}(y_k = 0) = \mathbb{P}(C_k = 0) = \exp(-\lambda)$. Conversely, when $C_k > 0$, y_k is deduced from the sum of C_k independent Gamma random variables. For clarity, following the work of Zhou et al. (2022a),

we re-parameterize the TD distribution, setting $\theta = \mu^{1-\rho}/(1-\rho)$ and $\kappa(\theta) = \mu^{2-\rho}/(2-\rho)$. This results in the revised TD distribution as:

$$f_{\text{TD}}(y_k|\theta, \phi) = f_{\text{TD}}(y_k|\mu, \phi, \rho) = a(y_k, \phi, \rho) \exp \left[\frac{1}{\phi} \left(y_k \frac{\mu^{1-\rho}}{1-\rho} - \frac{\mu^{2-\rho}}{2-\rho} \right) \right], \quad (6)$$

where

$$a(y_k, \phi, \rho) = \begin{cases} 1 & \text{if } y_k = 0, \\ \frac{1}{y_k} \sum_{j=1}^{\infty} \frac{y_k^{-j\alpha} (\rho-1)^{\alpha j}}{\phi^{j(1-\alpha)} (2-\rho)^j j! \Gamma(-j\alpha)} & \text{if } y_k > 0. \end{cases} \quad (7)$$

In this case, μ, ϕ , and ρ are the three parameters governing the probability and expected value of traffic incident risk. The parameters in Gamma and Poisson distributions $(\lambda, \alpha, \gamma)$ can be obtained as (Kurz, 2017; Halder et al., 2019; Mallick et al., 2022), :

$$\lambda = \frac{1}{\phi} \frac{\mu^{2-\rho}}{2-\rho}, \quad \alpha = \frac{2-\rho}{\rho-1}, \quad \gamma = \phi(\rho-1)\mu^{\rho-1}. \quad (8)$$

Generally, the TD is favoured because of its congruity with the nature of road risk, defined as an expectation derived from three categories of severity and their associated frequencies. This echoes the empirical observation that traffic incident frequency aligns with a Poisson distribution, while incident severity follows a Gamma distribution characterized by zero inflation and long tails. A significant departure from previous studies such as STZINB-GNN, our approach to the TD distribution innovatively parameterizes ϕ to model the left-skewed zero- or minor-risk situations, and ρ to address the issues related to the long tail. This nuanced approach enables a more realistic modelling of the incident risk landscape, providing improved prediction accuracy and a better understanding of the complex dynamics of road risk.

3.2.2. ZITD Distribution

Traffic risk values often exhibit a characteristic abundance of zero values, as depicted in the numerical analysis. This surplus often surpasses the zero input expected in conventional models, thus risking the oversight of many hazardous road situations due to methodological constraints. Likewise, while the standard TD model proposed in section 3.2.1 accommodates a positive probability density at zero, as illustrated by $\mathbb{P}(y_k = 0) = \mathbb{P}(C_k = 0) = \exp(-\lambda)$, it encounters performance shortfalls when the empirical distribution of risk data at a road-level is exceedingly imbalanced and dominated by zero risk values (Mallick et al., 2022; Zhou et al., 2022a).

To address this issue, we introduce a refinement to the model, known as the Zero-Inflated Four-parametric Tweedie Compound (ZITD) model. To our knowledge, this marks the inaugural application of a ZITD distribution along with its estimation framework for the traffic incident domain, specifically tailored for the characterization of road-level traffic risk. In the construction of the ZITD distribution, we integrate a sparsity parameter, denoted as π , to account for the skewness inherent in risk data, often manifested as an excess of zeros. This sparsity parameter π is utilized to denote a zero-inflation scenario, while the probability $1 - \pi$ corresponds to the TD distribution:

$$y_k = \begin{cases} 0 & \text{with probability } \pi \\ Y & \text{with probability } 1 - \pi, Y \sim f_{\text{TD}}(Y|\mu, \phi, \rho) \end{cases} \quad (9)$$

Finally, by denoting the ZITD model as $y_k \sim f_{\text{ZITD}}(\pi, \mu, \phi, \rho)$, we formulate the probability density function of this model as follows:

$$f_{\text{ZITD}}(y_k|\pi, \mu, \phi, \rho) = \begin{cases} \pi + (1 - \pi)f_{\text{TD}}(y_k = 0|\mu, \phi, \rho) & \text{if } y_k = 0 \\ (1 - \pi)f_{\text{TD}}(y_k|\mu, \phi, \rho) & \text{if } y_k > 0 \end{cases} \quad (10)$$

In accordance with this specification, we tackle the problem of extreme zero inflation by applying a linear weighting to the zero value, such that $\mathbb{P}(y_k = 0) = \pi + (1 - \pi) \exp(-\frac{1}{\phi} \frac{\mu^{2-\rho}}{2-\rho})$. It's important to note that this probability is significantly higher than the probability of observing a zero count from the TD distribution. Its increased probability intuitively signifies zero inflation. This modification ensures that the mean value of the ZITD distribution is $\mathbb{E}(y_k) = (1 - \pi)\mu$.

In the proposed ZITD model, each of the four parameters plays a critical role in managing various facets of road-level incident risk values. Importantly, the sparsity parameter, π , modulates the weights for situations devoid of risk occurrence. This modulation leads to a significant reformation of the dispersion parameter, ϕ , which is now interpreted as weighted, thereby refining the model's approach towards left-skewed scenarios. In this capacity, larger ϕ values symbolize an enhanced model ability to simulate instances predominantly characterized by none- or lower-risk situations. Complementing these, the index parameter ρ becomes instrumental for scenarios characterized by a long-tail distribution of road-level risk values. Higher ρ values, particularly those closer to 2, represent an enhanced capability to accommodate such instances, distinguishing this model from others that predominantly focus on mean values, represented by μ .

These parameters improve the model's representational capacity and deepen understanding of uncertainty quantification for predicted outcomes. By moving beyond point estimation to interval estimation, the ZITD model marks a significant advancement in road risk representation and prediction.

3.3. The framework of Spatiotemporal Zero-Inflated Tweedie Graph Neural Networks (STZITD-GNNs)

In relation to the four parameters π, μ, ϕ, ρ of the ZITD probability distributions detailed above, we have designed a probabilistic spatiotemporal graph learning module, named STZITD-GNNs. This module extracts the spatiotemporal correlations $\mathcal{Z} = \mathcal{ST}_\Theta(X_{1:t}, Y_{1:t}, A)$ under the ZITD assumption for each road's risk and predicts future outcomes for the subsequent p time windows through $f_{ZITD}(X_{t+1:t+p}|\mathcal{Z})$. As described in Equation 11, the comprehensive probabilistic Spatiotemporal Graph Neural Network is denoted as \mathcal{ST}_Θ . It jointly takes historical spatiotemporal features, corresponding incident risk values, and the adjacency matrix as inputs, learning the parameter embedding \mathcal{Z} for future risk predictions.

$$\begin{aligned} f_{ZITD}(Y_{t+1:t+p}|\pi_{t+1:t+p}, \mu_{t+1:t+p}, \phi_{t+1:t+p}, \rho_{t+1:t+p}) \\ = f_{ZITD}(Y_{t+1:t+p}|\mathcal{ST}_\Theta(X_{1:t}, Y_{1:t}, A)) = f_{ZITD}(X_{t+1:t+p}|\mathcal{Z}). \end{aligned} \quad (11)$$

As illustrated in Figure 1, instead of conducting two independent estimations, our methodology commences with the deployment of a GRU acting as the temporal encoder. Subsequently, a GAT is implemented for the purpose of spatial encoding. The combined output from the GRU and GAT is utilized to parameterize the ZITD distribution. The proposed unified approach is formulated as showcased in Equation 12. Our architecture's encoding component applies a spatiotemporal embedding scheme complemented with an extra sparsity parameter and distribution parameters. On the other hand, the decoding component is responsible for probabilistic estimations of future risk values, which can be construed as the parameter set of the future risk distribution. In contrast with the principles of variational autoencoders (VAEs) (Kipf and Welling (2016b); Hamilton (2020)), which constraint the latent embedding with specific distributions such as Gaussian and t- distributions for a more robust representation of latent variables, we echo the statistical domain by allowing the integration of deep learning methodologies into parameters learning:

$$\pi_{t+1:t+p}, \mu_{t+1:t+p}, \phi_{t+1:t+p}, \rho_{t+1:t+p} = \mathcal{ST}_\Theta(X_{1:t}, Y_{1:t}, A). \quad (12)$$

In the following sections, we present our STZITD-GNNs learning framework in greater detail. Firstly, we introduce the temporal encoder, GRU, and then delve into the crucial aspects of the spatial encoder, GAT.

3.3.1. Temporal encoder – GRU

Traffic incidents demonstrate significant temporal correlation, underscoring the idea that the dynamic temporal features of roads encapsulate a wealth of information. This observation has been acknowledged and exploited in prior methodologies (Wang et al., 2021a; Zhao et al., 2019). As shown in Figure 1, to seize these temporal proximity features, we implement a GRU (Chung et al., 2014). The GRU, in comparison to traditional LSTM networks, offers the advantage of learning relatively long-term dependencies without facing issues of vanishing and exploding gradients. In the GRU framework, there isn’t a segregation of internal and external states, as seen in LSTM networks. Instead, it addresses the gradient vanishing and exploding problem by directly integrating a linear dependency between the current network state h_t and the preceding state h_{t-1} . Consequently, while a GRU preserves the capabilities of an LSTM network, its architecture remains more streamlined (Gu et al. (2019); Mahmoud et al. (2021); Ma et al. (2022)).

Specifically, this component accommodates the feature sequence over past time windows $1:t$, thereby learning temporal dependencies. We represent the temporal embedding as \mathcal{Z}_T , taking into account both historical spatiotemporal road features and traffic risks as input:

$$\mathcal{Z}_T = \text{GRU}(X_{1:t}, Y_{1:t}), \quad (13)$$

Once the input features have been processed via the GRU, we obtain historical temporal embeddings \mathcal{Z}_T for all roads. These are subsequently directed to graph neural encoders. The GRU, in particular, consists of two gates: the update gate and the reset gate. The encoder processes a single input X_t, Y_t at time slot t and prior hidden features h_{t-1} in sequence:

$$\begin{aligned} r_t &= \sigma(W_r \cdot [h_{t-1}, X_t, Y_t] + b_r), \\ u_t &= \sigma(W_u \cdot [h_{t-1}, X_t, Y_t] + b_u), \\ \tilde{h}_t &= \tanh(W_c \cdot [r_t \cdot h_{t-1}, X_t, Y_t] + b_c), \\ h_t &= (1 - u_t) \cdot h_{t-1} + u_t \cdot \tilde{h}_t \end{aligned} \quad (14)$$

In the equation above, h_t and h_{t-1} represent hidden features at the current and preceding time steps, respectively, while \tilde{h}_t denotes the candidate state that temporarily stores information from reset and update gates (r_t, u_t). The variables W and b (i.e. $W_r, W_u, W_c, b_r, b_u, b_c$) represent learnable weight and bias matrices, respectively. Importantly, r_t acts as the reset gate, determining the extent of integration of hidden features from previous time steps into features at the current time step. Meanwhile, u_t serves as the update gate, controlling how much information from previous time steps will be carried over to the next time step. The $\tanh(\cdot)$ is the hyperbolic tangent function. We perform the GRU gate operations step by step and select the final layer’s hidden features h_t as the temporal embedding $\mathcal{Z}_T \in \mathbb{R}^{N \times F}$, where F denotes the dimension of road temporal embedding.

3.3.2. Spatial encoder – GAT

Within our research, road data is fundamentally perceived as having an inherent graph structure. This perspective facilitates the interpretation of node features as graph signals. To accommodate such graph-structured information, we employ the GAT (Veličković et al., 2017), an effective methodology renowned for enabling potential model deepening while concurrently incorporating dynamic spatial correlation into our network, achieved through real-time adjustment of attention weights in response to data changes (Wang et al., 2022b; Zhang et al., 2019a).

Distinct from GCN of a spectral-domain convolution (Kipf and Welling, 2016a), GAT operates as a spatial-domain convolutional network. Instead, GAT emphasizes the magnitude of the graph signal value at distinct points and their inter-distance to execute the convolution process. This trait empowers GAT to alleviate the over-smoothing issue associated with GCN deepening, thereby augmenting prediction precision regarding peaks and valleys (Zhao et al., 2019).

Initially, we compute the attention coefficient α_{ij} between roads v_i and v_j as per the following equation:

$$\alpha_{ij} = \frac{\exp(\text{LeakyReLU}(\vec{a}^T [W_a \mathcal{Z}_i || W_a \mathcal{Z}_j]))}{\sum_{A_{i,o} > 0} \exp(\text{LeakyReLU}(\vec{a}^T [W_a \mathcal{Z}_i || W_a \mathcal{Z}_o]))}, \quad (15)$$

In this equation, $A_{i,o} > 0$ represents the neighbourhood or connected roads of the road v_i . $W_a \in \mathbb{R}^{F \times F'}$ and $\vec{a} \in \mathbb{R}^{2F'}$ are learnable weights, where F' denotes the hidden dimension. We apply the concatenation function $[||\cdot]$ to concatenate the embedding of v_i and its neighbours, utilizing learnable parameter W_a and mapping function \vec{a} . Subsequently, we employ an activation function, $\text{LeakyReLU}(\cdot)$, and normalize the attention coefficient α_{ij} using the $\exp(\cdot)$ function. The embedding of road v_i is consequently updated with a linear combination of the neighbourhood of road v_i and itself, wherein these computed attention coefficients are employed.

In order to preemptively address potential inaccuracies in attention assignments, we have incorporated multiple attention assignments, otherwise known as multiple attention heads, into our approach. This tactic greatly amplifies the expressive capacity of the model. The multi-head attention mechanism facilitates concurrent consideration of information from a wide range of representation subspaces at various positions. This enables each head to learn and focus on different facets of the input data, thereby enhancing the model's ability to comprehend and accurately represent the data (Reza et al., 2022; Tang and Zeng, 2022; Ding et al., 2023). Herein, M symbolizes the number of attention mechanisms, with the output embeddings from these mechanisms being concatenated in the following manner:

$$\mathcal{Z}_i = ||_{m=1}^M \sigma \left(\sum_{A_{i,j} > 0} \alpha_{ij}^m W_a^m \mathcal{Z}_{T_j} \right), \quad (16)$$

In this equation, superscript m denotes a different head. The embedding of the road v_i is optimized by aggregating its neighbours' embedding with attention coefficients α_{ij}^m , and we apply learnable weights W_a^m for different heads. After this, we apply a nonlinear sigmoid function and concatenate different heads of embedding. The multi-head attention mechanisms hereby ensure stability in the attention mechanisms learning process and encapsulate diverse perspectives of road-level graph features. Notably, in Eq 16, the dimension of the output feature is $M \times F'$, rather than F' . To ensure consistency in the output feature's dimension, we compute the average of each road's embedding in the last layer as follows:

$$\mathcal{Z}_i = \sigma \left(\frac{1}{M} \sum_{m=1}^M \sum_{A_{i,j} > 0} \alpha_{ij}^m W_a^m \mathcal{Z}_{T_j} \right). \quad (17)$$

Finally, we input temporal embedding \mathcal{Z}_T into GAT to capture spatial dependency and obtain spatiotemporal $\mathcal{Z}_i \in \mathbb{R}^{F'}$ of road v_i . After that, we use \mathcal{Z} to infer the four-parameter STZITD-GNNs model.

3.3.3. Parameter Decoders

To transmute the acquired spatiotemporal embeddings into ZITD parameter values, we have devised four parameter decoders to operate on \mathcal{Z} . Consequently, four parameters, namely $\pi_{t+1:t+p}$, $\mu_{t+1:t+p}$, $\phi_{t+1:t+p}$, and $\rho_{t+1:t+p}$ can be computed from \mathcal{Z} , as detailed below:

$$\begin{aligned}\pi_{t+1:t+p} &= \sigma(W_\pi \cdot \mathcal{Z} + b_\pi) \\ \mu_{t+1:t+p} &= \text{ReLU}(W_\mu \cdot \mathcal{Z} + b_\mu) \\ \phi_{t+1:t+p} &= \text{ReLU}(W_\phi \cdot \mathcal{Z} + b_\phi) + \epsilon \\ \rho_{t+1:t+p} &= \sigma(W_\rho \cdot \mathcal{Z} + b_\rho) + 1 + \epsilon\end{aligned}\tag{18}$$

Here, π lies within the range of $[0, 1]$, μ falls within the interval $[0, +\infty)$, ϕ exists within $(0, +\infty)$, and ρ spans the range of $(1, 2)$. The learnable weight matrices are represented as $W_\pi, W_\mu, W_\phi, W_\rho, b_\pi, b_\mu, b_\phi, b_\rho \in \mathbb{R}^{F' \times p}$. $\lim \epsilon \rightarrow 0$ represents the smallest value, and $\text{ReLU}(\cdot)$ signifies the ReLU activation function.

3.4. Learning Framework of STZITD-GNNs

3.4.1. ZITD Loss Function

As previously mentioned, our encoding mechanism employs a spatiotemporal embedding architecture complemented by a sparsity parameter. On the other hand, the decoding component involves probabilistic estimation of future road traffic risks. To accurately predict these risks, the overall learning objective can be seen as maximizing the log-likelihood function: $\max \log f_{ZITD}(y_k | \pi, \mu, \phi, \rho)$. We utilize the negative likelihood as our loss function to better fit the distribution into the data. Here, y denotes the ground-truth values corresponding to one of the predicted risks with parameters π, μ, ϕ, ρ . The log-likelihood of ZITD is composed of the $y = 0$ and $y > 0$ parts:

For $y > 0$, $NLL_{y>0} = -\log f_{ZITD}(y > 0 | \pi, \mu, \phi, \rho)$:

$$\begin{aligned}\log f_{ZITD}(y > 0 | \pi, \mu, \phi, \rho) &= \log(1 - \pi) + \log f_{TD}(y > 0 | \mu, \phi, \rho) \\ &= \log(1 - \pi) + \frac{1}{\phi} \left(y \frac{\mu^{1-\rho}}{1-\rho} - \frac{\mu^{2-\rho}}{2-\rho} \right) + \log a(y > 0, \phi, \rho) \\ &= \log(1 - \pi) + \frac{1}{\phi} \left(y \frac{\mu^{1-\rho}}{1-\rho} - \frac{\mu^{2-\rho}}{2-\rho} \right) - \log y + \log \sum_{j=1}^{\infty} \frac{y^{-j\alpha} (\rho - 1)^{\alpha j}}{\phi^{j(1-\alpha)} (2-\rho)^j j! \Gamma(-j\alpha)} \\ &\geq \log(1 - \pi) + \frac{1}{\phi} \left(y \frac{\mu^{1-\rho}}{1-\rho} - \frac{\mu^{2-\rho}}{2-\rho} \right) - \log(j_{max} \sqrt{-\alpha} y) + j_{max}(\alpha - 1).\end{aligned}\tag{19}$$

In this equation, $j_{max} = \frac{y^{2-\rho}}{(2-\rho)\phi}$ and $\alpha = \frac{2-\rho}{1-\rho} < 0$. We optimize the lower bound, hence $NLL_{y>0}$ can be optimized in this manner.

For $y = 0$, $NLL_{y=0} = -\log f_{ZITD}(y = 0 | \pi, \mu, \phi, \rho)$:

$$\begin{aligned}\log f_{ZITD}(y = 0 | \pi, \mu, \phi, \rho) &= \log(\pi) + \log(1 - \pi) f_{TD}(y = 0 | \mu, \phi, \rho) \\ &= \log(\pi) + \log(1 - \pi) + \frac{1}{\phi} \left(-\frac{\mu^{2-\rho}}{2-\rho} \right)\end{aligned}\tag{20}$$

Here, π, μ, ϕ, ρ are chosen and calculated in accordance with the index of $y = 0$ or $y > 0$. The ultimate negative log-likelihood loss function is given by:

$$NLL_{STZITD} = NLL_{y=0} + NLL_{y>0} + \eta \Theta^2.\tag{21}$$

Model parameter Θ can be optimized by minimizing the negative log-likelihood loss: $\hat{\Theta} = \text{argmin} NLL_{STZITD}$. η stands for the weight parameter for L_2 Normalization.

It's worth noting that our model can be extended to other distributions by modifying the probability layer to fit other distributions. The main reason is that we learn the parameters that determine distributions. For instance, if we choose the Gaussian distribution, we can parameterize the probability layer using the spatiotemporal embedding of the mean and variance, thereby quantifying the data uncertainty that follows the Gaussian distribution. By leveraging the flexibility of the probability layer, we design a range of benchmark models for comparison to the STZITD-GNNs model. Our code is available on Github ¹.

3.4.2. Time analysis & Training algorithms

We summarize the training procedure of STZITD-GNNs in Algorithm 1. Based on that, the time complexity can be analyzed as follows (for the sake of simplicity, we denote the hidden union of embedding $F' \approx F$ and F as F):

- For temporal encoders, the time complexity can be formulated as $O(tN(dF + F^2 + F))$.
- For spatial encoders, we assume the number of road edges to be $|E|$. Hence, when implementing the graph attention encoder, the complexity of computing attention becomes $O(M|E|F)$. Furthermore, when executing W_a multiplication, the cost is $O(MNF^2)$. This leads to a total time complexity of $O(M|E|F + MNF^2)$.
- When generating the four parameters, the four one-layer MLPs require a time complexity of $O(F^2p)$.

Algorithm 1 The training of STZITD-GNNs.

Require: Spatiotemporal road feature $X \in \mathbb{R}^{N \times T \times d}$, road network graph $G = (V, E, A)$, roads traffic risk $Y \in \mathbb{R}^{N \times T}$, model hyper-parameters M, F', F , and total time slot T , time window t, p .

- 1: Calculate road traffic risk Y via Eq. (1).
 - 2: Initialize parameters Θ via Xavier Initializer.
 - 3: **while** STZITD-GNNs is not converged **do** ▷ Train
 - 4: Calculate temporal embedding Z_T via Eq. (14) by road feature $X_{1:t}$; ▷ Temporal Encode
 - 5: Calculate spatiotemporal embedding Z via Eq. (17) by graph G and Z_T ; ▷ Spatial Encode
 - 6: Obtain four parameters $\pi_{t+1:t+p}, \mu_{t+1:t+p}, \phi_{t+1:t+p}, \rho_{t+1:t+p}$ via output layer refer to Eq. (18);
 - 7: Calculate distribution $f_{ZITD}(y_{t+1:t+p} | \pi_{t+1:t+p}, \mu_{t+1:t+p}, \phi_{t+1:t+p}, \rho_{t+1:t+p})$ from four parameters via Eq. (10);
 - 8: Minimizing negative log-likelihood loss NLL_{STZITD} against $Y_{t+1:t+p}$ via Eq. (21) using Adam Optimizer;
 - 9: **end while**
 - 10: End optimizing model parameters Θ ;
-

4. Experiments

In this section, we present a thorough evaluation of the proposed STZITD-GNNs model, employing real traffic incident data from three of London's most perilous boroughs in 2019: Lambeth, Tower Hamlets, and Westminster. Our evaluation is designed to examine the model's generalizability using two distinct types of input data: 14 days of historical data for 14-day (Long-term) predictions, and 7 days of historical data for 7-day

¹<https://github.com/STTDAnonymous/STTD>

(Short-term) predictions. Our evaluations focus on two aspects: firstly, to illustrate the ability of our proposed model to effectively quantify the uncertainty of road-level traffic incident data, and secondly, to showcase its accuracy in comparison to several relevant baseline models.

We initiate our discussion by presenting our datasets (Section 4.1), followed by an outline of the experimental setup (Section 4.2). Next, we introduce the evaluation metrics (Section 4.3) and baseline models (Section 4.4) utilized in our study. Subsequently, we delve into a comparison of our model’s performance against alternative methods (Section 4.5), rounded off with a discussion on supplementary experiments as sensitive analysis (Section 4.6).

4.1. Data Description

In this study, we utilize the real-world UK road incidents and safety statistics, known as STATS19, to validate our model. The STATS19 dataset, maintained by the Department for Transport in the UK, is comprised of three interlinked tables providing information about incidents, their severity, and related vehicle data ².

The case study of our research is in three boroughs within Greater London, UK: Westminster, Lambeth, and Tower Hamlets, as shown in Figure 2. These boroughs were selected due to their notable high frequency of incidents from January to December 2019. The detailed statistics for these areas are summarized in Table 3. Upon examination of these three boroughs—which boast the highest number of incidents on an average of 3 to 5 incidents per day—it’s evident that the zero rates remain considerably high, even after factoring in the spatial spillover effects. This pattern arises due to the substantial number of road nodes present in these boroughs. Despite the relatively frequent occurrence of incidents, a significant proportion of roads experience no incidents, resulting in a high zero rate. Furthermore, an examination of the risk value frequency distribution presented in Figure 3 reveals not only the presence of a zero-inflated issue but also a clear long-tail effect. Remember that The long-tail effect refers to a particular type of distribution of variables where a larger share of occurrences are far away from the "head" or central part of the distribution and are spread out, forming a "long tail". The data distributional pattern from Figure 3 indicates that while the majority of risk values are quite low (equating to 1), the frequency of occurrence decreases as the risk level increases. Consequently, these conditions make the dataset particularly suited for the application of our proposed model.

To assess the generalization ability of our model, it is imperative to consider the unique geospatial aspects of each borough within Greater London. These 32 local authority districts, along with the City of London, constitute the administrative area of Greater London, England. Each borough is governed by a separate London borough council and exhibits distinct socio-demographic characteristics, road network formats, and transport risk patterns, adding layers of complexity to the urban risk prediction task (Dixit and Sivakumar, 2020; Yuan et al., 2018). By including boroughs of differing characteristics in our validation, we strive to demonstrate the broad applicability of the STZITD-GNNs model.

Table 3: The statistics of Westminster, Lambeth, and Tower Hamlets datasets.

Dataset	Roads/Nodes	Edges	Features	incident Counts	Zero-Inflated
Westminster ¹	4,822	20,128	110	1,745	95.72%
Lambeth ¹	5,659	21,574	110	1,335	96.71%
Tower Hamlets ¹	4,688	17,928	110	1,236	96.28%

¹ <https://roadtraffic.dft.gov.uk/downloads>

²<https://www.gov.uk/guidance/road-incident-and-safety-statistics-guidance>

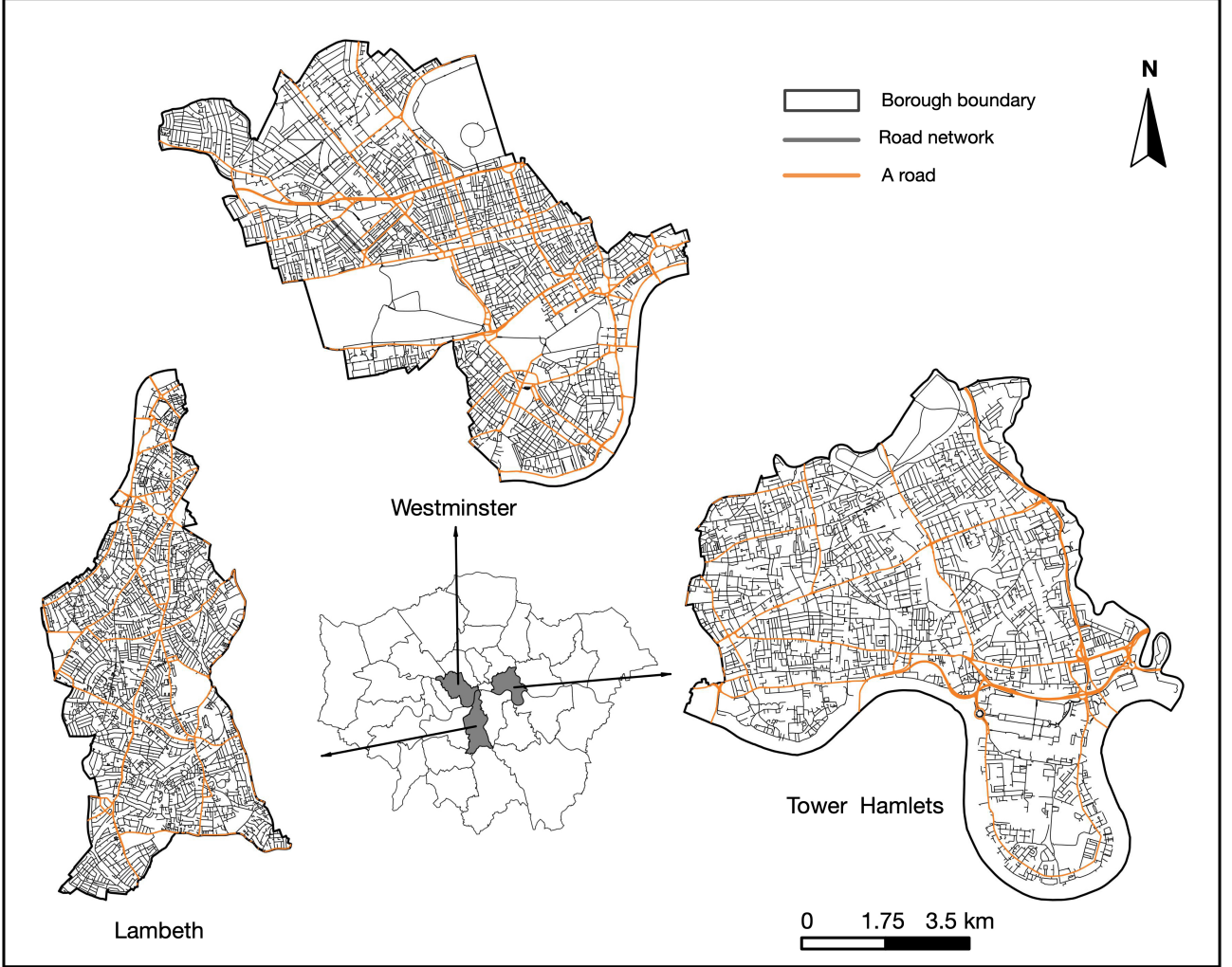


Figure 2: The map of three boroughs, London

4.2. Experiment Setup

The parameters of STZITD-GNNs are optimized with Adam optimizer Kingma and Ba (2014), where the learning rate is set to 0.01, and weight decay is 0.01. In STZITD-GNNs, $N_{epoch} = 20$, the hidden unit is set to 42, GAT head is set to 3. The parameters of baselines are optimized using the Adam Kingma and Ba (2014) with L_2 regularization and a dropout rate of 0.2. The GNNs in STZITD-GNNs and baselines are all two-layered. We set the hidden units to 42 as well. Similar to previous work, we also employ the early-stopping strategy with patience equals 10 to avoid over-fitting.

STZITD-GNNs is implemented in Pytorch 1.9.0 with Python 3.8. All the experiments are conducted on 1 NVIDIA GeForce RTX 3090, 24 GB. All baselines are implemented by ourselves.

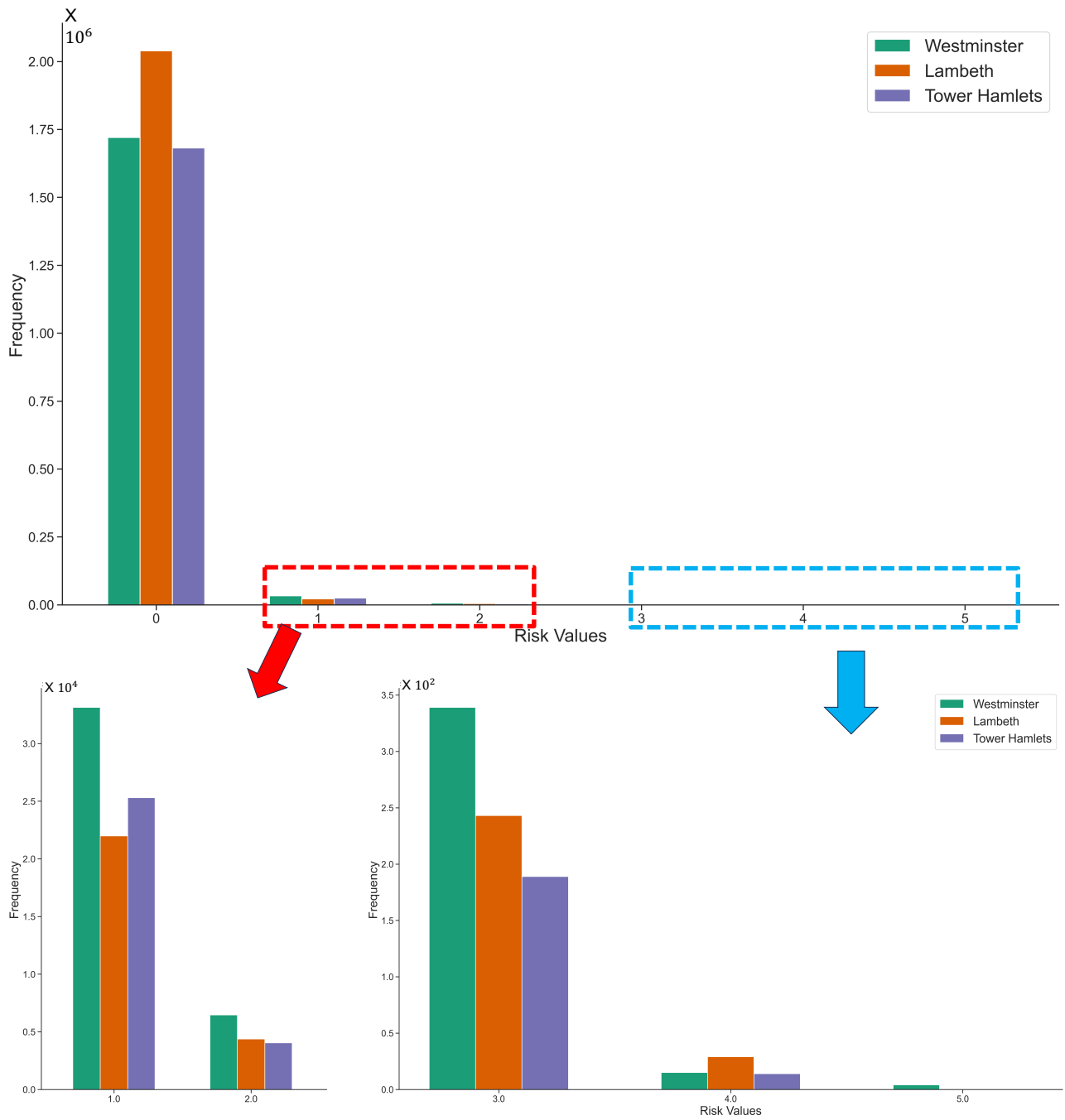


Figure 3: The distribution of Risk values frequency in the three boroughs, London. Both zero-inflated issue and long-tail effect are significant in the data distributions.

4.3. Evaluation Metrics

We use eight metrics to evaluate the performance of our STZITD-GNNs from four aspects, including the predictive regression effect of road incident risk, the predictive effect of distributional characteristics, the degree of zero inflation fit, and the hit rate of high-risk roads.

4.3.1. Accuracy Metrics

For the point estimate aspect, we compare the numerical value prediction. For probabilistic distribution outputs like our model, we use the mean value of the distribution as the numerical output. For specific metrics, we use Mean Absolute Error (MAE), Mean Absolute Percentage error (MAPE), and Root Mean Squared Error (RMSE) to evaluate the predicted risks of all roads. Specific definitions are summarized:

$$\begin{aligned} \text{MAE} &= \frac{1}{pN} \sum_{j=1}^p \sum_{i=1}^N |y_{ij} - \hat{y}_{ij}|, \\ \text{MAPE} &= \frac{1}{pN} \sum_{j=1}^p \sum_{i=1}^N \left| \frac{y_{ij} - \hat{y}_{ij}}{y_{ij}} \right|, \\ \text{RMSE} &= \sqrt{\frac{1}{pN} \sum_{j=1}^p \sum_{i=1}^N (y_{ij} - \hat{y}_{ij})^2}, \end{aligned} \tag{22}$$

where \hat{y}_{ij} and y_{ij} are the predicted (i.e. distribution mean) and ground-truth values of i^{th} road at time slot j^{th} respectively. Literally, $p = 14$ or 7 days, and time slot j^{th} is inside this predicted window. Lower values of these metrics mean better performance.

4.3.2. Uncertainty Quantification Metric

To assess the measured uncertainty, we utilize a selection of metrics: Kullback-Leibler Divergence (KLD), Mean Prediction Interval Width (MPIW), and Prediction Interval Coverage Probability (PICP) predicated on a 5%-95% confidence interval with a confidence level set at 5% ($\alpha = 5\%$). The KLD is deployed to gauge the degree of similarity between the output distribution generated by our model and the distribution of the test set. Concurrently, the MPIW serves as a tool to determine the mean width of the prediction interval, with its output heavily contingent upon the distinct traits of the distribution. It's optimal for the values of MPIW and KLD to be as small as possible. The PICP, on the other hand, is implemented to evaluate whether the ground-truth value, denoted as y_{ij} , lies within the predicted interval. A higher PICP is regarded as more advantageous. It is important to recognize the inherent trade-off between PICP and MPIW: an ideal prediction interval would be both narrow and cover a substantial portion of the data points. However, a wider MPIW naturally leads to a larger PICP. This interaction poses a considerable challenge for any model that is designed to cater to more precise assumptions, as elucidated in Wang et al. (2023a) and Zhu et al. (2022).

$$\begin{aligned}
\text{KLD} &= \frac{1}{pN} \sum_{j=1}^p \sum_{i=1}^N (\hat{y}_{ij} \log \frac{\hat{y}_{ij} + \epsilon}{y_{ij} + \epsilon}), \\
\text{MPIW} &= \frac{1}{pN} \sum_{j=1}^p \sum_{i=1}^N (U_{ij} - L_{ij}), \\
\text{PICP} &= \frac{1}{pN} \sum_{j=1}^p \sum_{i=1}^N \mathcal{I}(U_{ij} < \hat{y}_{ij} < L_{ij}),
\end{aligned} \tag{23}$$

since many y_{ij} and \hat{y}_{ij} values are likely to be zeros, a minimum value $\epsilon = 10^{-5}$ is used to avoid numerical issues because of division by 0. Since the KLD measures the difference between two distributions, smaller values are desirable. Moreover, L_{ij} and U_{ij} correspond to the lower and upper bound of the confidence interval for observation road i at time slot j^{th} . Indicate function $\mathcal{I}(U_{ij} < \hat{y}_{ij} < L_{ij})$ equals 1 if the condition is true, else 0.

4.3.3. Zero Inflated Metrics

Given the notable data sparsity issue, as evident in Figure 3, it becomes crucial to assess the proficiency of models in capturing these zero entries. To evaluate the model's performance on the discrete road risk entries, we leverage the true-zero rate (ZR) measurements. The ZR acts as a quantifier of how well the model mirrors the sparsity observed in the ground-truth data. A ZR score value closer to the ground-truth zero-inflated ratios signifies superior model performance. The mathematical expression for the ZR is given as:

$$\text{ZR} = \frac{1}{pN} \sum_{j=1}^p \sum_{i=1}^N \mathcal{I}(y_{ij} = 0 \cap \hat{y}_{ij} < \epsilon), \tag{24}$$

where the indicator function, $\mathcal{I}(y_{ij} = 0 \cap \hat{y}_{ij} < \epsilon)$, equals 1 if the condition holds true, and 0 otherwise. We set a limit approaching zero ($\epsilon \rightarrow 0$) as the threshold and consider $\hat{y}_{ij} < \epsilon$ as equivalent to zero.

4.3.4. Hit Rate Metric

In order to evaluate the proficiency of our model in identifying roads with increased incident risk, we utilize the Average Hit Rate (HR) metric. This metric assesses the model's performance by determining the fraction of risk scenarios accurately flagged within the top a percent of locations predicted to bear the highest incident probability. In particular, we scrutinize the top 20% ($a = 20\%$) of high-risk road length coverage and ascertain whether these roads indeed exhibit a high risk with actual incidents transpiring at these specific locales and times (Zhang and Cheng, 2020; Zhang et al., 2019b). By correlating high-risk forecasts with actual incidents, $HR(a)$ serves as a robust gauge of our model's predictive precision for areas demonstrating a heightened incident risk. The mathematical expression for HR is given as:

$$HR(a) = \frac{1}{p} \sum_{j=1}^p \frac{\sum_{i=1}^N \mathcal{I}(y_{ij} > 0 \cap \hat{y}_{ij} \geq \text{Top}(\hat{y}_{:j}, a))}{\sum_{i=1}^N \mathcal{I}(y_{ij} > 0)}, \tag{25}$$

The indicator function, $\mathcal{I}(y_{ij} > 0 \cap \hat{y}_{ij} \geq \text{Top}(\hat{y}_{:j}, a))$, equals 1 if the condition is satisfied, and 0 otherwise. $\mathcal{I}(y_{ij} > 0) = 1$ if an incident occurs, and it equals 0 otherwise. In this context, $y_{ij} > 0$ denotes that an incident indeed transpired on the i^{th} road during the j^{th} time slot, indicated by a non-zero risk value. Conversely, $\text{Top}(\hat{y}_{:j}, a)$ represents the boundary value corresponding to the top a percentage of predicted risk levels for all road length coverage at the j^{th} time slot.

4.4. Baseline Models

The following baselines are considered in our comparative evaluation of our proposed model, including the mean-predict method (HA), spatial-temporal graph deep learning methods such as STGCN and STGAT, parameterization models such as STG, STNB, STTD and STZINB:

- **HA**(Liu and Guan (2004)): Historical Average serves as the statistic baseline. It is calculated by averaging the road traffic risks in the same time intervals from the historical data to predict one step ahead of future road traffic risk.
- **STGCN**(Yu et al. (2018)): Spatiotemporal Graph Convolution Network, which utilizes graph convolution and 1D convolution to capture spatial dependencies and temporal correlations, respectively.
- **STGAT**(Velićković et al. (2017)): Graph Attention Network is able to attend over their neighbourhoods' features, specifying different weights to different nodes in a neighbourhood. We replace GCN with GAT in STGCN and call this STGAT.
- **STG-GNNs**(Wang et al. (2023a)): Same as STZITD-GNNs, we replace the statistical assumption of road traffic risks with Gaussian Distribution instead.
- **STNB-GNNs**(Zhuang et al. (2022)): Same as STZITD-GNNs, we replace the statistical assumption of road traffic risks with Negative Binomial Distribution instead.
- **STTD-GNNs**: Same as STZITD-GNNs, we replace the statistical assumption of road traffic risks with TD Distribution instead.
- **STZINB-GNNs**(Zhuang et al. (2022)): Same as STZITD, we replace the statistical assumption of road traffic risks with Zero-Inflated Negative Binomial Distribution instead.

4.5. Performance Comparison

A series of experiments were executed to accomplish the task of quantifying uncertainty in road-level traffic incident risk across three diverse datasets under two scenarios: long-term and short-term. The experimental results encompassing the performance evaluation of our proposed model, STZITD-GNNs, and the existing baselines are displayed in Tables 4 and 5. The tabulated results use a colour-coded scheme to aid interpretation, with the red and blue zones highlighting the best and second-best performance scores, respectively. The direction of the vectors serves to visually represent the comparative performance of the STZITD-GNNs, depicting whether it surpasses (upward vector) or lags behind (downward vector) the best scores of the baseline models.

In terms of predictive accuracy, it is evident that our STZITD-GNNs model consistently outperforms the baselines in the majority of scenarios. This superiority is especially pronounced in the context of long-term prediction. When juxtaposed with the second-best baseline model, the accuracy improvements offered by our model span from 11.15% to 38.34% in terms of MAE, 10.16% to 49.06% for MAPE, and a substantial 9.08% to 34.60% for RMSE. This applies to both long-term and short-term prediction in node estimation tasks. It is worth noting that STZITD-GNNs shares similar spatiotemporal graph neural network structures as STG-GNNs, STNB-GNNs, STZINB-GNNs, and STTD-GNNs. The consistently superior results demonstrate the efficacy of adopting the ZITD distribution, which, due to its distinct characteristics, is able to capture the nuances of the ground truth data more comprehensively.

In terms of the uncertainty quantification task, the STZITD-GNNs model outstrips all baseline models for long-term prediction. This provides robust evidence that our model exhibits superior capacity in capturing

long-term spatiotemporal dependencies compared to short-term prediction. The STTD-GNNs model closely follows STZITD-GNNs in the PICP metric for the Lambeth and Westminster datasets in short-term prediction scenarios. Moreover, the STZITD-GNNs model delivers a substantial performance uplift in the KLD metric. Particularly in zero-inflated situations, the STZITD-GNNs model excels at modelling zero-risk roads, presenting improvements ranging from 12.60% to 24.11% across all tested scenarios. STZITD-GNNs also outperform the baselines in HR (20%), underscoring its capability to accurately identify high-incident risk roads and offer valuable preventive recommendations. Consequently, integrating the sparsity parameter π bolsters the model’s ability to handle the excessive zeroes in the data, enabling it to form more accurate prediction confidence intervals.

An intriguing observation from the experimental results is the relatively comparable performance of STTD-GNNs and STZINB-GNNs to the STZITD-GNNs model. These models incorporate both temporal dependencies and spatial relations and account for the zero-inflated parameters. While STZINB-GNNs showcase superior performance in uncertainty quantification owing to its explicit modelling of the zero-inflated parameter, STTD manages to outperform STZINB in other metrics. This can be attributed to STTD-GNNs’s unique ability to address both the long-tail problem as well as the zero-inflated issue. However, it tends to struggle with extremely zero-inflated data. Contrarily, the HA model, which neglects spatial dependencies, yields the poorest performance when compared to STGCN and STGAT. This emphasizes the indispensability of considering spatial and temporal dependencies for spatial-temporal prediction tasks.

We must acknowledge the well-documented trade-off between PICP and MPIW, as discussed in Section 4.3.2. However, our STZITD-GNNs model, by integrating the zero-inflation parameter π into the traditional TD, and transforming it into a ZITD, remarkably manages to alleviate this trade-off. The zero-inflation component of the ZITD plays a pivotal role in this context as it effectively captures the substantial proportion of zero-valued (non-risk) roads in the dataset. This enhances the model’s ability to represent the true distribution of road risks more accurately, which, in turn, facilitates the formation of narrower prediction intervals for a majority of cases, thus lowering the MPIW. Concurrently, the model retains its capacity to encompass a substantial proportion of the data points, thereby maintaining a high PICP. This dual ability of the STZITD-GNNs model significantly mitigates the traditionally challenging trade-off between MPIW and PICP, which considerably boosts the model’s overall predictive performance. Additionally, it enhances the model’s capacity to effectively capture and represent the complexity and characteristics of the urban road-level risk data.

In summary, the four-parameter STZITD-GNNs model emerges as the best-performing model, outperforming the three-parameter models such as STTD-GNNs and STZINB-GNNs, as well as the two-parameter models and single-parameter methods like STGCN and STGAT. These plots provide insights into how the STZITD-GNNs model effectively learns and adjusts the TD distribution parameters to cater to the characteristics of urban traffic risk data. Experiment results underscore the robustness of our proposed STZITD-GNNs model and its ability to effectively quantify uncertainty in road-level traffic incident risk.

4.5.1. Visualization of Predicted Road-Level Risk

To illustrate the practical implications of our STZITD-GNNs model, we have generated choropleth maps that visually represent road-level risks across three distinct boroughs over two separate time windows. These maps are presented in Figure 4, which depicts risks over a long-term period of 14 days, and Figure 5, which captures risks over a short-term period of 7 days. Each borough encompasses unique risk patterns, which are juxtaposed against our model’s predicted traffic risk values to provide a comprehensive perspective of its predictive capacity.

Upon examination of these visualizations, our model’s high predictive accuracy is notably consistent across both the 7-day and 14-day time windows. It accurately identifies roads with a range of risk levels, as well as

Table 4: Comparison of Long-Term (14-day) Prediction Performance Across Three Boroughs. Red shading indicates the best-performing model, while blue signifies the second-best. To maintain clarity, detailed names of all GNNs in the final five statistical-integrated deep learning models are omitted. Instead, abbreviations such as STG, STNB, STTD, STZINB, and STZITD are used to underscore the most significant modifications within the GNN models.

Metric	Model	HA	STGCN	STGAT	STG	STNB	STTD	STZINB	STZITD
Dataset		Lambeth							
ACC	MAE	0.1348	0.0613	0.0302	0.1182	0.0802	0.0315	0.0544	0.0238 \uparrow 21.19%
	MAPE	0.4142	0.4023	0.3203	0.4046	0.0363	0.0426	0.0265	0.0135 \uparrow 49.06%
	RMSE	0.2107	0.1436	0.1122	0.1827	0.1390	0.1098	0.1191	0.0947 \uparrow 13.75%
Uncertainty	KLD	0.2691	0.1068	0.0512	0.5039	1.5580	0.0849	0.2596	0.0248 \uparrow 51.56%
	MPIW(a=5%)	/	/	/	0.4871	0.1946	0.1349	0.0454	0.0204 \uparrow 55.07%
	PICP(a=5%)	/	/	/	0.7328	0.8903	0.9873	0.9796	0.9899 \uparrow 00.26%
Zero Inflated	ZR	0.5203	0.5305	0.5986	0.1992	0.5621	0.6838	0.6408	0.7870 \uparrow 15.09%
Hit Rate	HR(20%)	0.4520	0.6113	0.6422	0.2666	0.4471	0.7123	0.6184	0.7659 \uparrow 07.39%
Dataset		Tower Hamlets							
ACC	MAE	0.0939	0.2385	0.0305	0.1741	0.2475	0.0433	0.2135	0.0271 \uparrow 11.15%
	MAPE	0.2896	0.2017	0.1205	0.2662	0.0399	0.0246	0.0594	0.0221 \uparrow 10.16%
	RMSE	0.1987	0.1325	0.1355	0.3896	0.1548	0.1186	0.1368	0.0918 \uparrow 22.60%
Uncertainty	KLD	0.2888	0.0612	0.0319	0.8090	1.9791	0.1096	0.6278	0.0132 \uparrow 58.62%
	MPIW(a=5%)	/	/	/	0.5321	0.2263	0.0810	0.0296	0.0156 \uparrow 47.30%
	PICP(a=5%)	/	/	/	0.6439	0.9442	0.9845	0.9845	0.9871 \uparrow 00.26%
Zero Inflated	ZR	0.4998	0.4896	0.5234	0.1351	0.5158	0.6420	0.7526	0.8876 \uparrow 17.94%
Hit Rate	HR(20%)	0.4752	0.5869	0.6950	0.2647	0.5022	0.6368	0.5827	0.7224 \uparrow 03.94%
Dataset		Westminster							
ACC	MAE	0.1467	0.0784	0.0847	0.1055	0.3266	0.0579	0.3240	0.0357 \uparrow 38.34%
	MAPE	0.1884	0.8976	0.6012	2.9295	0.0330	0.0973	0.0415	0.0259 \uparrow 21.52%
	RMSE	0.5999	0.2384	0.2433	0.6681	0.2909	0.1552	0.2751	0.1015 \uparrow 34.60%
Uncertainty	KLD	0.4149	0.2218	0.2626	2.6582	2.3624	0.1452	0.3889	0.0331 \uparrow 77.20%
	MPIW(a=5%)	/	/	/	0.8542	0.6272	0.2021	0.0493	0.0259 \uparrow 47.46%
	PICP(a=5%)	/	/	/	0.6036	0.9363	0.9801	0.9796	0.9893 \uparrow 00.94%
Zero Inflated	ZR	0.5981	0.1431	0.2922	0.2071	0.5393	0.5079	0.6288	0.7328 \uparrow 16.54%
Hit Rate	HR(20%)	0.4217	0.5020	0.4808	0.2933	0.4503	0.6075	0.5139	0.6898 \uparrow 13.55%

those with negligible risk, across all three boroughs. A particularly striking instance of this precision is the model’s predictions for the Westminster borough, an area characterized by a lower zero-inflation rate and a more dense graph structure.

Long-term risk representations, as seen in Figure 4, offer a robust overview of the risk landscape. They enable the identification of a larger set of risk-prone roads with remarkable accuracy. This reiterates the model’s capacity to leverage long-term data effectively, enhancing its predictive strength. However, it is also evident that there are opportunities for improvement, particularly in predicting zero-risk roads. In the cases of Lambeth and Tower Hamlets, the model occasionally identifies zero-risk roads as low-risk. While these errors predominantly fall within the lower-risk category and do not greatly impact the identification of the highest-risk roads, addressing this can help further refine the model’s performance.

Figure 5 showcases the model’s capacity to effectively highlight high-risk and zero-risk roads, despite the

Table 5: Comparison of Short-Term (7-day) Prediction Performance Across Studied Boroughs. Red shading indicates the best-performing model, while blue signifies the second-best. To maintain clarity, detailed names of all GNNs in the final five statistical-integrated deep learning models are omitted. Instead, abbreviations such as STG, STNB, STTD, STZINB, and STZITD are used to underscore the most significant modifications within the GNN models.

Metric	Model	HA	STGCN	STGAT	STG	STNB	STTD	STZINB	STZITD
Dataset		Lambeth							
ACC	MAE	0.1339	0.0815	0.0316	0.0482	0.1051	0.0378	0.0774	0.0249 _{↑21.20%}
	MAPE	0.4848	0.3553	0.2025	0.4427	0.0781	0.0495	0.0245	0.0213 _{↑13.06%}
	RMSE	0.2377	0.1712	0.1084	0.1847	0.1715	0.1151	0.1398	0.0978 _{↑09.78%}
Uncertainty	KLD	0.2641	0.1561	0.0628	0.5218	0.7585	0.1031	0.4734	0.0291 _{↑54.66%}
	MPIW(a=5%)	/	/	/	0.4920	0.2296	0.1170	0.0070	0.0098 _{↑40.00%}
	PICP(a=5%)	/	/	/	0.6944	0.8897	0.9807	0.9874	0.9908 _{↑00.34%}
Zero Inflated	ZR	0.5031	0.3610	0.6359	0.1023	0.5177	0.6506	0.5797	0.7611 _{↑16.98%}
Hit Rate	HR(20%)	0.4432	0.5462	0.6592	0.3006	0.4417	0.6867	0.5749	0.7364 _{↑07.24%}
Dataset		Tower Hamlets							
ACC	MAE	0.1957	0.0375	0.0398	0.0997	0.1159	0.0547	0.0827	0.0311 _{↑17.07%}
	MAPE	0.4997	0.4860	0.2405	0.4542	0.0509	0.0574	0.0562	0.0423 _{↑16.90%}
	RMSE	0.2258	0.1273	0.1319	0.2811	0.1013	0.1261	0.1219	0.0921 _{↑09.08%}
Uncertainty	KLD	0.2680	0.0596	0.0704	0.3696	0.7678	0.1322	0.4842	0.0155 _{↑73.99%}
	MPIW(a=5%)	/	/	/	0.5688	0.1223	0.0918	0.0052	0.0043 _{↑17.31%}
	PICP(a=5%)	/	/	/	0.6218	0.9250	0.9450	0.9748	0.9887 _{↑01.43%}
Zero Inflated	ZR	0.4943	0.5417	0.5132	0.0890	0.5219	0.6052	0.6886	0.8546 _{↑24.11%}
Hit Rate	HR(20%)	0.4693	0.6123	0.5661	0.2919	0.4882	0.6150	0.6021	0.6885 _{↑11.95%}
Dataset		Westminster							
ACC	MAE	0.1448	0.0676	0.0673	0.4521	0.1874	0.0594	0.1295	0.0427 _{↑28.11%}
	MAPE	0.4473	1.0104	0.7151	2.3351	0.0388	0.1183	0.0569	0.0310 _{↑20.10%}
	RMSE	0.1504	0.2044	0.1985	0.6541	0.2175	0.1548	0.1573	0.1357 _{↑12.34%}
Uncertainty	KLD	0.4485	0.1789	0.1795	2.8741	0.9136	0.1595	0.7628	0.0628 _{↑60.63%}
	MPIW(a=5%)	/	/	/	0.8789	0.3813	0.1594	0.0032	0.0095 _{↓196.9%}
	PICP(a=5%)	/	/	/	0.5766	0.9151	0.9804	0.9762	0.9857 _{↑00.54%}
Zero Inflated	ZR	0.5340	0.2030	0.2439	0.2032	0.5091	0.5258	0.6112	0.6882 _{↑12.60%}
Hit Rate	HR(20%)	0.3827	0.5595	0.5274	0.2852	0.4456	0.6332	0.4859	0.6167 _{↓02.60%}

reduced 7-day input data window. The importance of this capacity cannot be understated, as it offers invaluable insights for transport officers and road users alike. These insights can be utilized to plan and prioritize mobility options to prevent unanticipated losses, even when only a week’s worth of data is available. Moreover, our model consistently and accurately identifies the spatial compactness (or connectedness) of high-risk roads across all three boroughs, irrespective of the prediction window. Although this was not a primary focus of our model, the detection of compactness can prove highly beneficial in practical contexts. Compact and connected high-risk roads can be patrolled more efficiently with limited resources, a fact that is echoed in previous studies Adepeju et al. (2016); Zhang and Cheng (2020).

In light of the impressive PSCP score exceeding 98%, as per Table 4 and Table 5, we confidently assert that the STZITD-GNNs model excels in predicting road-level risks through learning from historical spatiotemporal patterns. This proficiency persists despite the varying spatial patterns and daily road risk counts across the three boroughs, highlighting the model’s adaptability and robust performance across diverse contexts. This consistent accuracy underscores the model’s potential as a powerful instrument in urban risk management, capable of providing critical insights to guide both policy making and daily navigation decisions.

4.5.2. Hit Rate study under different coverage of the roads

Figure 6 presents a mean hit rate line chart, spanning the three boroughs under consideration, averaged over the entire testing period. In this depiction, the coverage of the road length gradually increases, extending up to 20%. On an overarching level, the STZITD-GNNs model maintains a high mean hit rate across varying incident scenarios, with a minor exception noted in the short-term predictive performance for Westminster. More specifically, the accuracy exceeds 80% until the coverage broadens to 20%, thereby underscoring the model’s consistent and dependable performance.

When drawing comparisons between the three boroughs, the parallels between short and long-term predictive hit rates are most prominent within the Tower Hamlets dataset. This resemblance could potentially be ascribed to the less sparse distribution of traffic incidents within this region over the testing period, thereby resulting in less pronounced variability in the predictions. Alternatively, the winter season, which overlaps with our testing period, could potentially bring about more sparse traffic incident scenarios in Westminster. Consequently, due to the scarcity of input information, the short-term predictions within this borough might be marginally affected, which is reflected in a slightly lower hit rate.

It is worth noting that the ability of the STZITD-GNNs model to maintain high predictive accuracy, even with the increasing coverage of the road length, indicates its capacity to efficiently handle larger spatial scales. This characteristic is particularly beneficial in practical applications, where the model may need to predict risks for extensive road networks. Moreover, the model’s resilience against changes in the spatiotemporal distribution of incidents demonstrates its adaptability to varying urban dynamics, further enhancing its applicability in real-world scenarios.

4.5.3. Comparative Analysis of UQ for Baseline Models and STZITD-GNNs Through a Time-wise MPIW Study

To evaluate the UQ performance of our STZITD-GNNs model in contrast to the baseline models, we conduct a time-wise study of the MPIW. This assessment is depicted in Figure 7 and Figure 8 and extends to each prediction step for both short and long-term predictions across the three boroughs. The objective is to establish an MPIW that is narrow yet encompasses a significant proportion of the test samples, consequently ensuring a robust and dependable prediction interval for traffic risk.

Our STZITD-GNNs model consistently narrows down the prediction intervals by dynamically fine-tuning the prediction interval in accordance with the risk particular to each road segment. This dynamism effectively

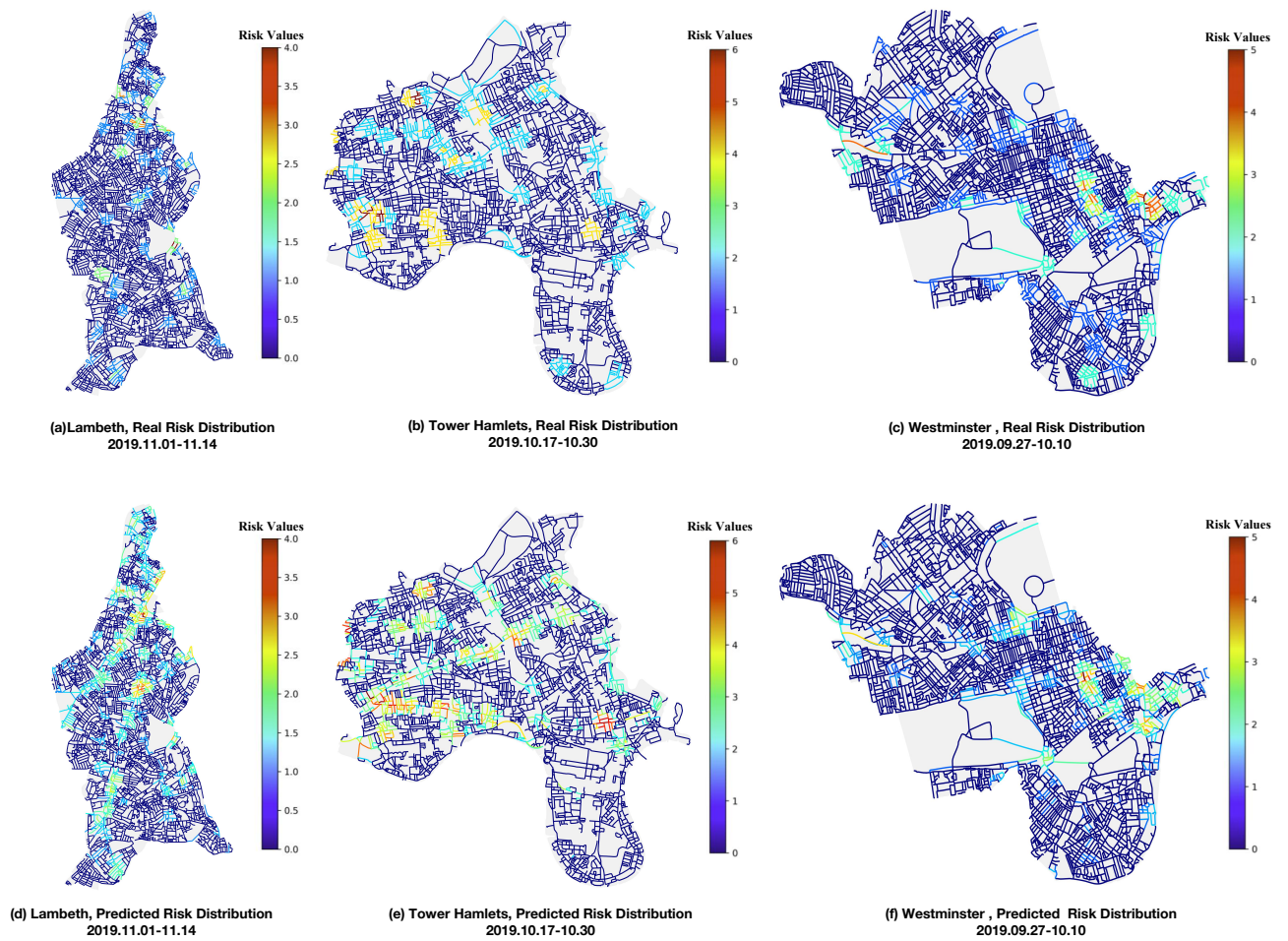


Figure 4: Predicted long-term (14-day) risk on Lambeth, Tower Hamlets, and Westminster.

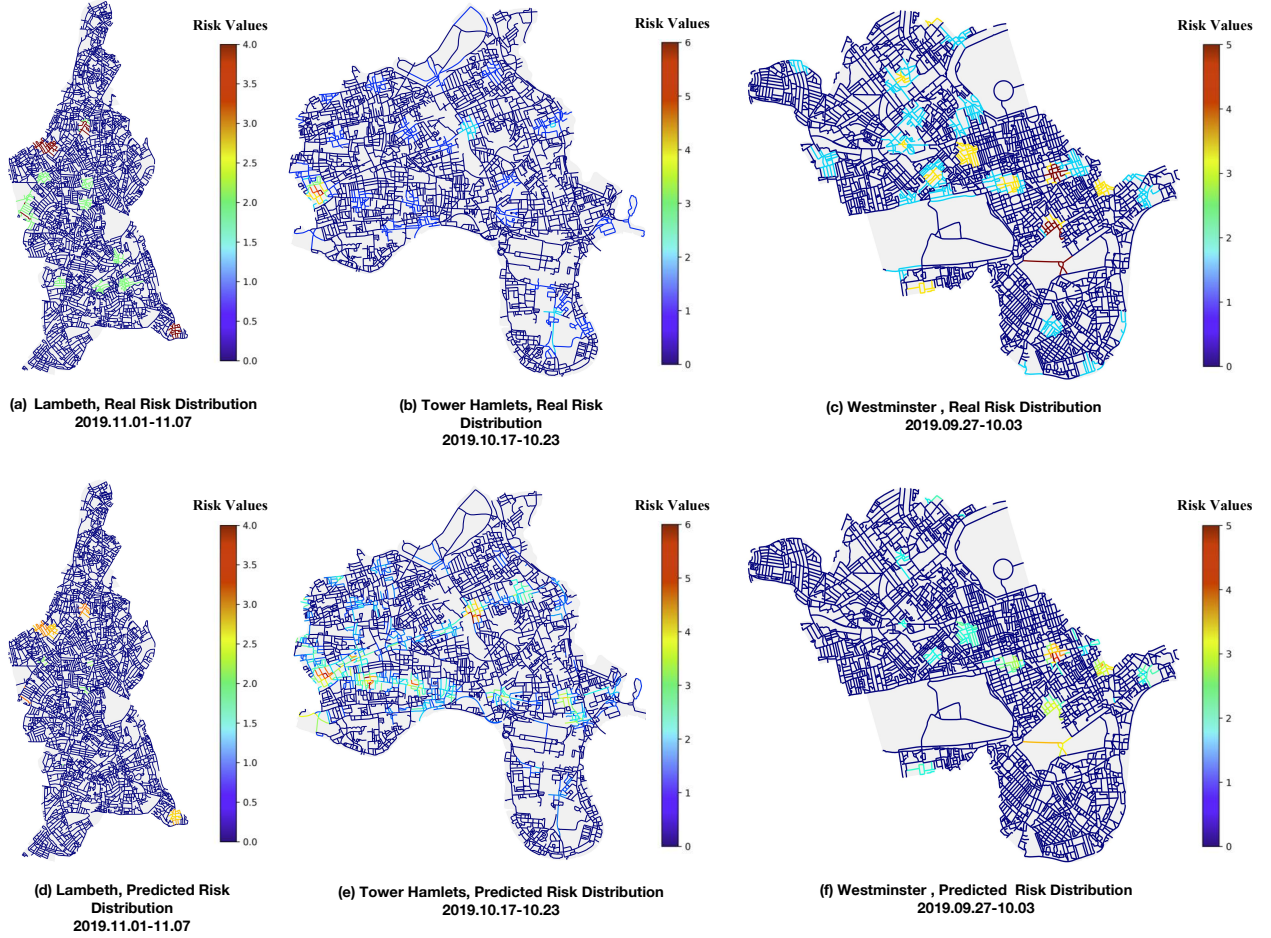


Figure 5: Predicted short-term (7-day) risk on Lambeth, Tower Hamlets, and Westminster.

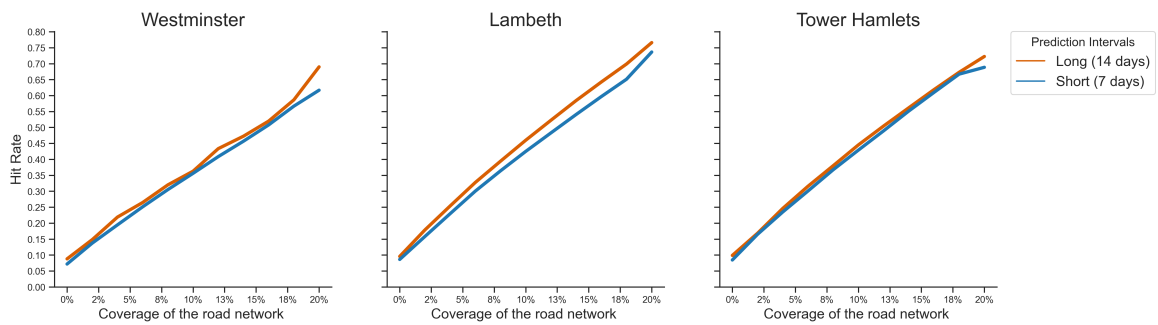


Figure 6: Hit rate increase figure under different road network coverage rates for long and short prediction intervals.

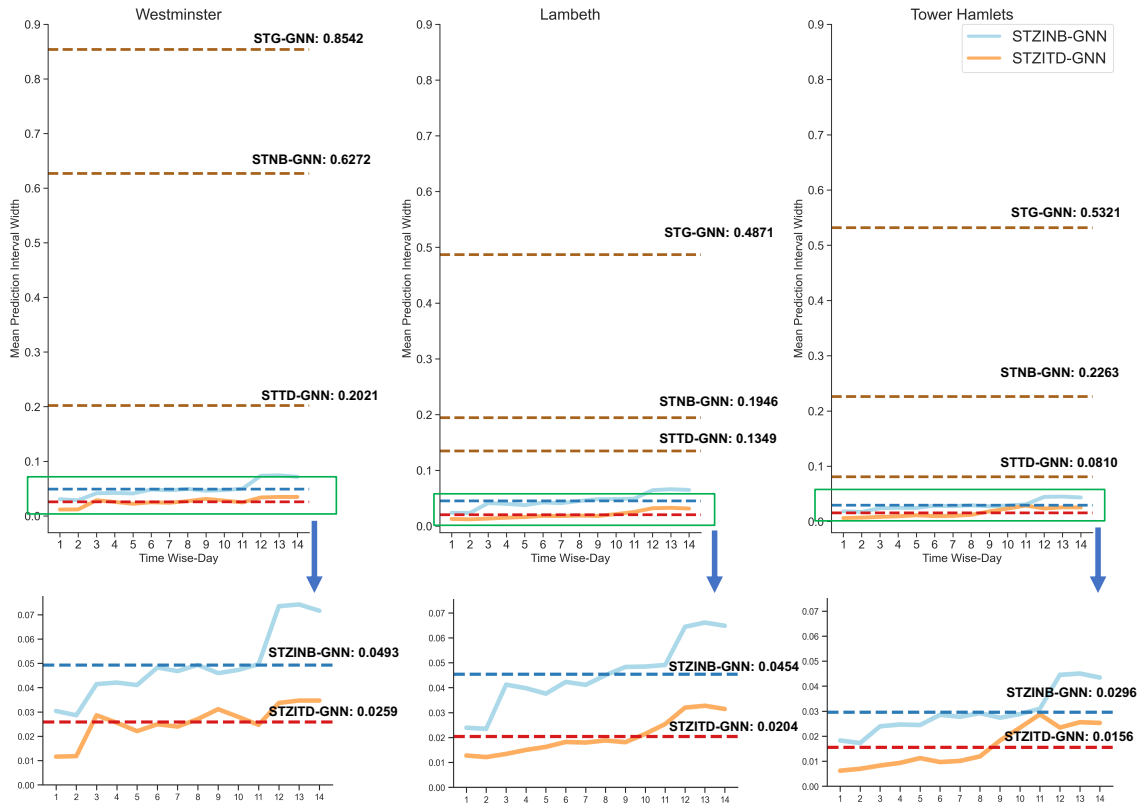


Figure 7: Time-wise MPIW changing lines for long intervals predictions for baselines and STZITD-GNNs.

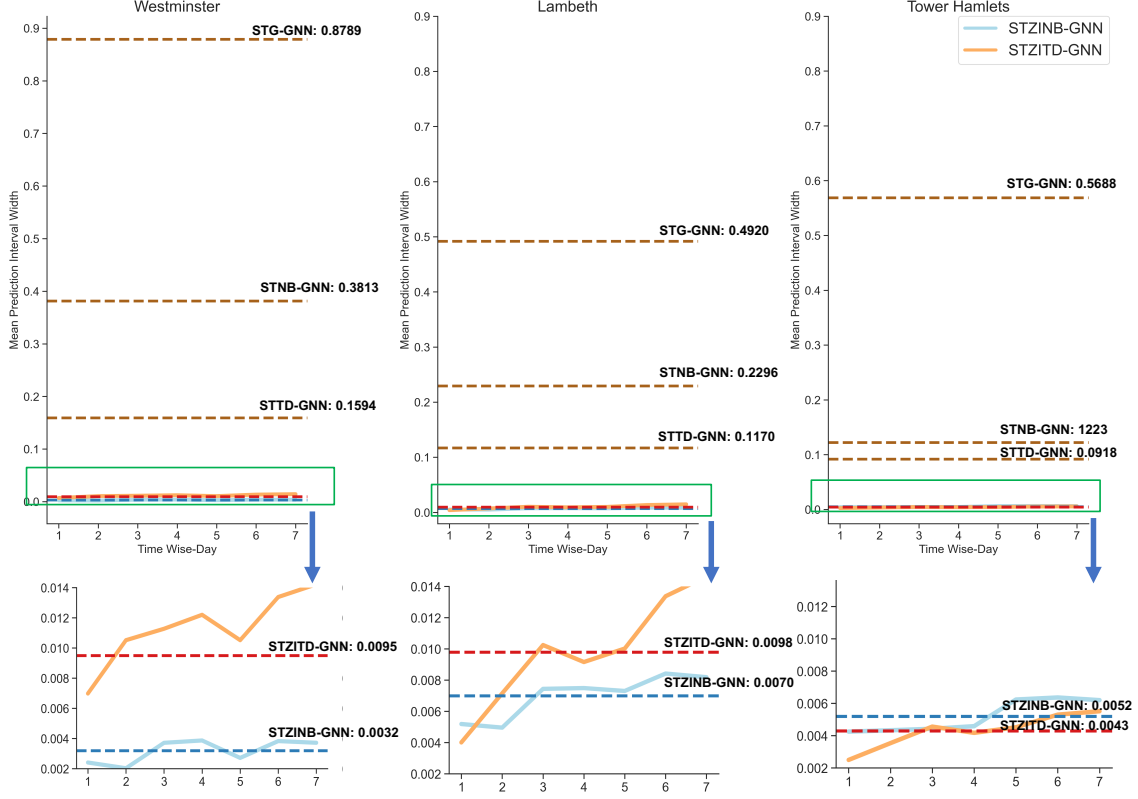


Figure 8: Time-wise MPIW changing lines for short intervals predictions for baselines and STZITD-GNNs.

allows the STZITD-GNNs model to outperform the baseline models in the majority of tasks. This success can be attributed to the enhanced proficiency of the ZITD model in handling overdispersed, zero-inflated urban road-level risk data, surpassing the capabilities of other distribution models.

The Gaussian and NB distributions have limitations in this context: Gaussian distributions often overlook the preponderance of zero values, while NB distributions concentrate only on the binary risk outcomes, thereby neglecting long-tail risk values. Both these shortcomings lead to a larger MPIW. While ZINB and ZITD both consider zero-value skewness, the ZITD distribution utilizes sparsity parameter π weighted dispersion parameter ϕ to map the substantial proportion of zero-valued (non-risk) roads and TD parameters to map low-risk roads as well as long-tail middle and high-risk roads. Thanks to its ability to capture the distinct characteristics of this complex road-level risk data distribution, it helps to mitigate overfitting to the data, leading to a narrower MPIW with a higher level of confidence.

Our analysis shows that the smallest MPIW typically occurs on the first testing day, followed by a rise over time. In figure 7, this temporal increase is less erratic in the long-term (14-day input) predictions compared to the baseline models. However, figure 8 exhibits noticeable fluctuations in both baseline models and STZITD-GNNs. This trend may reflect the inherent uncertainty and randomness of the risk situation with only a 7-day input period, resulting in less stability due to the limited spatiotemporal information.

Moreover, a fluctuating MPIW appears in the short-term predictions for Westminster and Lambeth, po-

tentially stemming from a higher prevalence of zero-risk values. This could introduce greater uncertainties for the prediction intervals (Zhuang et al., 2022), given the infrequent occurrence of traffic risks within the 7-day testing period, thereby augmenting prediction uncertainty. Nevertheless, the MPIW in these two regions is commensurate with that of the state-of-the-art STZINB-GNN model and is notably lower than other baseline models.

Though a larger MPIW can ensure a good coverage rate for the true risk values, it may also frequently underestimate or overestimate risk information, even when the model has relative confidence in the prediction (Wang et al., 2023a; Zhou et al., 2021). Thus, we recognize the merits of our proposed model in maintaining stability and reducing variance in predicted risk values at the road level. Notably, our model’s superior performance remains consistent across the three boroughs, demonstrating its adaptability to different road conditions, even under diverse spatiotemporal embeddings.

4.6. Sensitivity Analysis

4.6.1. Analysis of long-tail risk data characteristics

The long-tail effect is an integral attribute of data distribution, playing a key role in the selection of statistical components for traffic risk evaluation. To delve deeper into the influence of this long-tail effect on our model, we produce a four-dimensional 3D surface plot, as depicted in Figure 9. However, due to the inherent limitations of visualization techniques, representing all four parameters in a single five-dimensional plot is not feasible. Moreover, as the sparsity parameter π acts as a weight for the original TD parameters, we focus on the TD parameters (ϕ , ρ , μ) in our graphic representation. The points plotted to represent predicted risk values, while the actual risk values y are expressed through the colour bar in the plot.

Upon visualizing data across three boroughs under two temporal scenarios, it becomes clear that the learned ρ values exhibit a consistent trend towards larger values, often approaching 2. Furthermore, This pattern underscores our model’s capacity to capture the long-tail characteristic inherent in the risk distribution across diverse geographical and temporal contexts. This observed behaviour also stems from the inherent properties of the TD. Herein, ρ significantly influences the distribution’s dispersion, with larger ρ values denoting a heavier-tailed distribution, a characteristic that aligns well with our risk data’s long-tail nature. The increase in ρ can be considered an adaptive response to our loss function’s component, $y^{\frac{\mu^{1-\rho}}{1-\rho}} (y > 0)$. This component penalizes underestimations of true risk values situated within the long tail, thereby steering the model towards more accurate risk predictions within these zones.

Concurrently, we observe a marked increase in the ϕ values linked with zero-valued data, particularly pronounced in short-term scenarios. This can be attributed to the notably zero-inflated nature of urban risk data, characterized by significant segments of the road network without recorded incidents, a trait that becomes more apparent in short-term periods due to lower incident occurrence. As stated in the section 3.2.1. in the original TD distribution, the ϕ parameter, associated with the frequency of zero occurrences, is essential in addressing this zero-inflation. However, with the exceedingly imbalanced nature of our data, this parameter may not adequately capture the prevalence of zeros. Hence, in our ZITD model, the amplified ϕ , under the influence of the sparsity parameter π , skillfully accommodates this feature, leading to a more accurate depiction of the inherent sparsity and discrete uncertainty in road-level risk prediction.

Further scrutiny reveals that the model parameter μ , which serves as the mean of the predicted risk values, exhibits a colour distribution that is well-aligned with the real risk values y . This direct correspondence further underlines the model’s robust performance in mean point estimation, adding another layer of validation to the effectiveness of the STZITD-GNNs model within the sphere of urban risk prediction tasks. The discernible correlation between μ and y also testifies to the model’s capacity to seamlessly capture and adapt to the

subtleties and nuances of urban risk data. This observation further consolidates the argument for the adoption of the STZITD-GNNs model for urban risk prediction and underscores its efficacy in handling the complexity of the task.

4.6.2. Analyzing Risk Data Through Lower-Dimensional Representation

The Multidimensional Scaling (MDS) algorithm, which is employed for the purpose of data dimensionality reduction and visualization, affords us the ability to transform high-dimensional data into a lower-dimensional space (Wickelmaier, 2003). It achieves this while preserving the relative distances between individual data points. This particular algorithm permits the extraction of inherent structural information and latent relationships present within the dataset, thereby enabling an intuitive visual observation and subsequent analysis of the data. With this approach, we utilize the MDS algorithm to validate the efficacy of our model in capturing long-tail risk efficiently, by visualizing the learned node embeddings in a 2D space across six distinct scenarios.

For the purposes of our analysis, risks greater than 1 are regarded as a long-tail or high-risk road. We then visualize the learned spatiotemporal embedding \mathcal{Z} on the test set. A method’s representational ability is judged on its capacity to learn representative embeddings in which similar nodes map to proximate objects. As such, nodes that belong to the same class are expected to cluster together in the MDS representation. The outcomes of these visualizations are displayed in Figure 10.

Analysis of these six figures indicates that the long-tail class tends to be naturally clustered and embedded into the low-risk class. This phenomenon can be attributed to the risk spatial spillover effects, wherein adjacent roads may share similar embeddings, despite having differing risk levels. While the clusters of low-risk and high-risk spatiotemporal embeddings are distinctly separate, high-risk classifications are still discernible, particularly within the Westminster dataset. Both Lambeth and Tower Hamlets datasets continue to display spatial aggregations, signifying that our model effectively incorporates the severity of risk in its embeddings. These observations, taken together, suggest that our proposed methodology is capable of adequately capturing the long-tail risk within the data, thereby validating its effectiveness.

This ability of the STZITD-GNNs model to identify and distinctly represent various risk categories in the low-dimensional embedding space enhances its interpretability. It provides an intuitive way to explore and comprehend the high-dimensional spatiotemporal risk patterns, contributing towards its potential applicability in real-world urban risk prediction tasks. Furthermore, the distinct clustering of low-risk and high-risk road segments, despite the inherent spatial spillover effects, underlines the model’s resilience in capturing the nuances of the risk landscape.

5. Conclusion and Discussion

Road traffic incidents remain a significant obstacle to the sustainability of urban environments and the dependability of transportation systems (Yang et al., 2021; Zhou et al., 2020). These incidents not only endanger the safety of road users but also introduce complexities in resource allocation and the efficacy of transportation infrastructures, underscoring the necessity for marked enhancements in predictive methodologies. The urgency of this advancement extends beyond academic or economic boundaries; it is intimately tied to the preservation of human lives (Ibrahim et al., 2021). Given the comprehensive implications of these incidents, the development of models capable of delivering both precise and reliable predictions for practical applications has emerged as a pressing priority.

The current landscape of incident risk prediction methodologies, while providing insightful contributions, also exposes areas for improvement. Low-resolution models, often preferred for their computational efficiency, tend

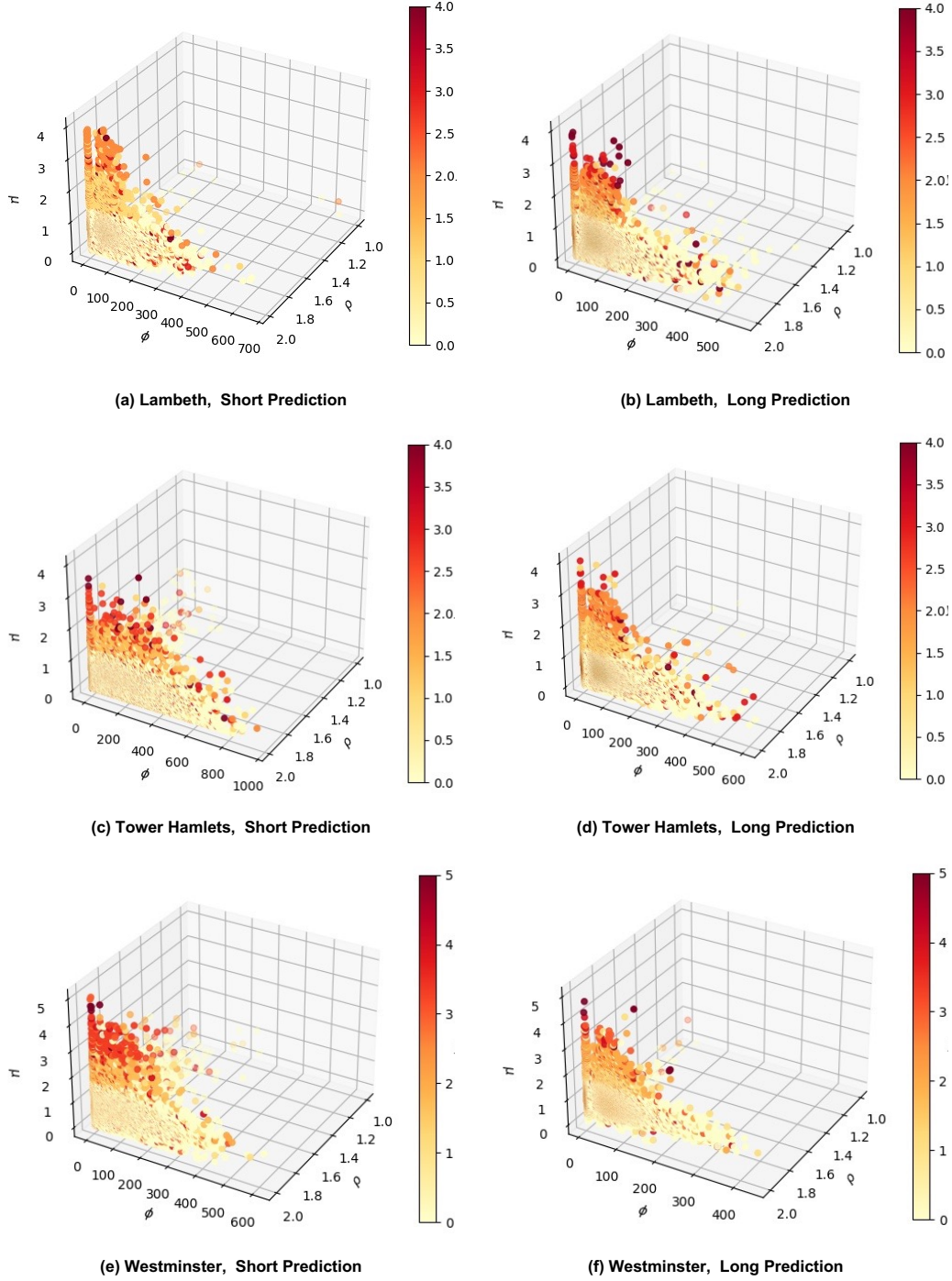


Figure 9: Three Tweedie parameters visualization on Lambeth, Tower Hamlet and Westminster with long (14 days) and short (7 days) predict. The colour bar shows the predicted risk values from highest to zero.

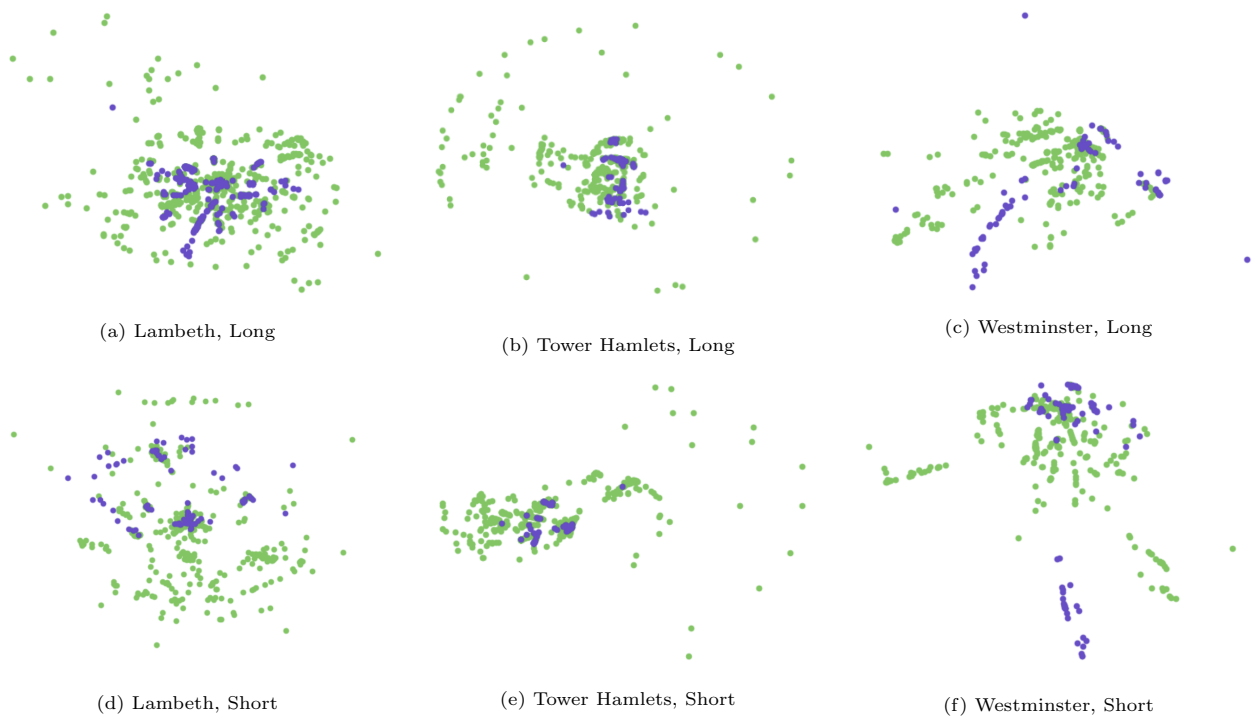


Figure 10: Low risk (green color) and high risk (blue color) spatiotemporal embedding \mathcal{Z} MDS-visualization on Lambeth, Tower Hamlets and Westminster with long (14 days) and short (7 days) predict.

to compromise on precision, leading to a high bias that may inhibit effective risk mitigation efforts. Additionally, frequency-based estimation techniques, while competent at pinpointing potential incident risks, often fall short in providing a complete representation of confidence in their predicted risk values, thus introducing a layer of uncertainty. Further, the distinct characteristic of traffic risk data, namely zero-inflation and overdispersion, is often inadequately addressed by conventional models when assimilating spatiotemporal risk features.

To address these gaps, we proposed the STZITD-GNNs model - a methodology purposefully designed to bridge the demand for high-resolution, road-level prediction and the requirement for rigorous uncertainty quantification. It takes into account the unique distribution attributes of risk data and, consequently, delivers predictions that are not only more precise and efficient, but also contributive to a nuanced understanding of uncertainties in traffic risks and the effectiveness of mitigation strategies. The primary contributions of this study are encapsulated in the following points:

- Guided by the overdispersed and zero-inflated nature of incident risk data, we extended the conventional TD Distribution to a ZITD. This extension enhanced the model’s ability to accurately capture the unique features of road-level incident risk data. By introducing a sparsity parameter, π , and especially integrating its effects into the dispersion parameter, ϕ , our model significantly bolsters its capacity to accurately depict the substantial proportion of zero-valued (non-incident) roads. Simultaneously, it assures a firm estimation of various risk levels, ranging from low-risk to long-tail middle and high-risk roads.
- Further, by integrating the ZITD encoder into the ST-GNNs, our model’s capabilities are significantly elevated from traditional prediction to pioneering UQ. This inventive amalgamation not only allows for effective capture of the complex spatiotemporal dynamics inherent to urban road-level risk but also adeptly transmits the distribution parameters to the output, thereby achieving superior mapping of output variance and intervals compared to traditional point estimation methodologies.
- The proposed model showcased remarkable predictive accuracy across three boroughs of London, underscoring its effectiveness across different urban environments, each exhibiting unique risk patterns. Notably, our model achieved high hit rates and ensured the greatest possible coverage of true risk values within its prediction intervals across diverse time windows and risk levels. This also underscores the model’s inherent resilience and adaptability across a range of risk scenarios.
- Lastly, our model adeptly handles the traditionally challenging trade-off between MPIW and PICP when mapping the UQ, providing both precise and confident risk predictions. By employing the zero-inflation component, it achieves narrower prediction intervals (reduced MPIW) while ensuring comprehensive coverage of actual risk data points (high PICP). This attribute makes our model particularly valuable for practical applications, where both precision and confidence in prediction intervals are critical.

The proposed STZITD-GNNs model, with its unique combination of spatial, temporal, and statistical modelling capabilities, provides a comprehensive and innovative solution for predicting and understanding urban road-level risks and the prediction of UQ.

While we are encouraged by the results of our current research, we also acknowledge that there remains scope for further refinement of our work. In our pursuit to map risk values more accurately, one of our future endeavours involves expanding the model’s applicability to different countries. Rather than adhering to the current individual training processes, we plan to develop a more versatile model that can be fine-tuned in response to geographic heterogeneities, thereby extending its transferable applicability to diverse areas.

Furthermore, we are keen to explore the integration of additional data sources into our model. Specifically, the incorporation of GPS data could provide valuable traffic exposure information, thereby further refining the risk predictions.

In our continued commitment to improving the accuracy and utility of our model, we also plan to evaluate our methodology using more comprehensive datasets. For example, incorporating urban characteristics extracted from street images or satellite imagery could enrich our model’s contextual understanding, potentially highlighting factors that exacerbate the impacts of traffic incidents in both spatial and temporal dimensions.

In conclusion, while we have made promising strides with the STZITD-GNNs model, we view this as the beginning of an ongoing journey towards perfecting urban road-level risk prediction. By continually refining our model and integrating new sources of data, we aim to provide a tool that can greatly assist in the mitigation of traffic risks and the enhancement of urban safety strategies worldwide.

6. Declaration of Generative AI and AI-assisted technologies in the writing process

During the preparation of this work the author(s) utilized GPT-4 for preliminary grammar checks and proofreading. After using this tool/service, the author(s) reviewed and edited the content as needed and take(s) full responsibility for the content of the publication.

References

- Abe, H. and Yadohisa, H. (2017). A non-negative matrix factorization model based on the zero-inflated tweedie distribution. *Computational Statistics*, 32(2):475–499.
- Adepeju, M., Rosser, G., and Cheng, T. (2016). Novel evaluation metrics for sparse spatio-temporal point process hotspot predictions—a crime case study. *International Journal of Geographical Information Science*, 30(11):2133–2154.
- Anderson, T. K. (2009). Kernel density estimation and k-means clustering to profile road accident hotspots. *Accident Analysis & Prevention*, 41(3):359–364.
- Bao, J., Liu, P., and Ukkusuri, S. V. (2019). A spatiotemporal deep learning approach for citywide short-term crash risk prediction with multi-source data. *Accident Analysis & Prevention*, 122:239–254.
- Barahimi, A. H., Eydi, A., and Aghaie, A. (2021). Multi-modal urban transit network design considering reliability: multi-objective bi-level optimization. *Reliability Engineering & System Safety*, 216:107922.
- Benlagha, N. and Charfeddine, L. (2020). Risk factors of road accident severity and the development of a new system for prevention: New insights from china. *Accident Analysis & Prevention*, 136:105411.
- Bergel-Hayat, R., Debbarh, M., Antoniou, C., and Yannis, G. (2013). Explaining the road accident risk: Weather effects. *Accident Analysis & Prevention*, 60:456–465.
- Bibri, S. E. (2018). A foundational framework for smart sustainable city development: Theoretical, disciplinary, and discursive dimensions and their synergies. *Sustainable Cities and Society*, 38:758–794.
- Caliendo, C., Guida, M., and Parisi, A. (2007). A crash-prediction model for multilane roads. *Accident Analysis & Prevention*, 39(4):657–670.
- Chakraborty, P., Hegde, C., and Sharma, A. (2019). Data-driven parallelizable traffic incident detection using spatio-temporally denoised robust thresholds. *Transportation research part C: emerging technologies*, 105:81–99.
- Chang, L.-Y. and Chen, W.-C. (2005). Data mining of tree-based models to analyze freeway accident frequency. *Journal of safety research*, 36(4):365–375.
- Chen, C., Fan, X., Zheng, C., Xiao, L., Cheng, M., and Wang, C. (2018). Sdcae: Stack denoising convolutional autoencoder model for accident risk prediction via traffic big data. In *2018 sixth international conference on advanced cloud and big data (CBD)*, pages 328–333. IEEE.
- Chen, Q., Song, X., Yamada, H., and Shibasaki, R. (2016). Learning deep representation from big and heterogeneous data for traffic accident inference. *Proceedings of the AAAI Conference on Artificial Intelligence*, 30(1).
- Chen, Y., Kang, Y., Chen, Y., and Wang, Z. (2020). Probabilistic forecasting with temporal convolutional neural network. *Neurocomputing*, 399:491–501.
- Cheng, T., Zhang, Y., and Haworth, J. (2022). Network spacetime ai: Concepts, methods and applications. *Journal of Geodesy and Geoinformation Science*, 5(3):78.
- Chong, M. M., Abraham, A., and Paprzycki, M. (2004). Traffic accident analysis using decision trees and neural networks. *arXiv preprint cs/0405050*.
- Chung, J., Gulcehre, C., Cho, K., and Bengio, Y. (2014). Empirical evaluation of gated recurrent neural networks on sequence modeling. *arXiv preprint arXiv:1412.3555*.
- Dai, L., Derudder, B., and Liu, X. (2018). The evolving structure of the southeast asian air transport network through the lens of complex networks, 1979–2012. *Journal of Transport Geography*, 68:67–77.
- Ding, C., Sun, S., and Zhao, J. (2023). Mst-gat: A multimodal spatial-temporal graph attention network for time series anomaly detection. *Information Fusion*, 89:527–536.
- Dixit, M. and Sivakumar, A. (2020). Capturing the impact of individual characteristics on transport accessibility and equity analysis. *Transportation research part D: transport and environment*, 87:102473.
- Dunn, P. K. (2004). Occurrence and quantity of precipitation can be modelled simultaneously. *International Journal of Climatology: A Journal of the Royal Meteorological Society*, 24(10):1231–1239.
- Gawlikowski, J., Tassi, C. R. N., Ali, M., Lee, J., Humt, M., Feng, J., Kruspe, A., Triebel, R., Jung, P., Roscher, R., et al. (2021). A survey of uncertainty in deep neural networks. *arXiv preprint arXiv:2107.03342*.
- Gu, Y., Lu, W., Qin, L., Li, M., and Shao, Z. (2019). Short-term prediction of lane-level traffic speeds: A fusion deep learning model. *Transportation research part C: emerging technologies*, 106:1–16.
- Guo, J., Huang, W., and Williams, B. M. (2014). Adaptive kalman filter approach for stochastic short-term traffic flow rate prediction and uncertainty quantification. *Transportation Research Part C: Emerging Technologies*, 43:50–64.
- Halder, A., Mohammed, S., Chen, K., and Dey, D. (2019). Spatial risk estimation in tweedie compound poisson double generalized linear models. *arXiv preprint arXiv:1912.12356*.
- Hamilton, W. L. (2020). Graph representation learning. *Synthesis Lectures on Artificial Intelligence and Machine Learning*, 14(3):1–159.
- He, W. and Jiang, Z. (2023). A survey on uncertainty quantification methods for deep neural networks: An uncertainty source perspective. *arXiv preprint arXiv:2302.13425*.
- Hossain, M. and Muromachi, Y. (2012). A bayesian network based framework for real-time crash prediction on the basic freeway segments of urban expressways. *Accident Analysis & Prevention*, 45:373–381.

- Hu, S.-R., Li, C.-S., and Lee, C.-K. (2010). Investigation of key factors for accident severity at railroad grade crossings by using a logit model. *Safety science*, 48(2):186–194.
- Huang, C., Zhang, C., Dai, P., and Bo, L. (2019). Deep dynamic fusion network for traffic accident forecasting. In *Proceedings of the 28th ACM international conference on information and knowledge management*, pages 2673–2681.
- Ibrahim, M. R., Haworth, J., Christie, N., Cheng, T., and Hailes, S. (2021). Cycling near misses: a review of the current methods, challenges and the potential of an ai-embedded system. *Transport reviews*, 41(3):304–328.
- Jiang, X., Zhuang, D., Zhang, X., Chen, H., Luo, J., and Gao, X. (2023). Uncertainty quantification via spatial-temporal tweedie model for zero-inflated and long-tail travel demand prediction. *arXiv preprint arXiv:2306.09882*.
- Jørgensen, B. (1987). Exponential dispersion models. *Journal of the Royal Statistical Society: Series B (Methodological)*, 49(2):127–145.
- Khosravi, A. and Nahavandi, S. (2014). An optimized mean variance estimation method for uncertainty quantification of wind power forecasts. *International Journal of Electrical Power & Energy Systems*, 61:446–454.
- Khosravi, A., Nahavandi, S., Creighton, D., and Atiya, A. F. (2010). Lower upper bound estimation method for construction of neural network-based prediction intervals. *IEEE transactions on neural networks*, 22(3):337–346.
- Kingma, D. P. and Ba, J. (2014). Adam: A method for stochastic optimization. *arXiv preprint arXiv:1412.6980*.
- Kipf, T. N. and Welling, M. (2016a). Semi-supervised classification with graph convolutional networks. *arXiv preprint arXiv:1609.02907*.
- Kipf, T. N. and Welling, M. (2016b). Variational graph auto-encoders. *arXiv preprint arXiv:1611.07308*.
- Koenker, R. and Hallock, K. F. (2001). Quantile regression. *Journal of economic perspectives*, 15(4):143–156.
- Kong, J., Fan, X., Jin, X., Lin, S., and Zuo, M. (2023). A variational bayesian inference-based en-decoder framework for traffic flow prediction. *IEEE Transactions on Intelligent Transportation Systems*.
- Kurz, C. F. (2017). Tweedie distributions for fitting semicontinuous health care utilization cost data. *BMC Medical Research Methodology*, 17:1–8.
- Laureshyn, A., de Goede, M., Saunier, N., and Fyhri, A. (2017). Cross-comparison of three surrogate safety methods to diagnose cyclist safety problems at intersections in norway. *Accident Analysis & Prevention*, 105:11–20.
- Li, R., Zhong, T., Jiang, X., Trajcevski, G., Wu, J., and Zhou, F. (2022a). Mining spatio-temporal relations via self-paced graph contrastive learning. In *Proceedings of the 28th ACM SIGKDD Conference on Knowledge Discovery and Data Mining*, pages 936–944.
- Li, R., Zhong, T., Jiang, X., Trajcevski, G., Wu, J., and Zhou, F. (2022b). Mining spatio-temporal relations via self-paced graph contrastive learning. In *Proceedings of the 28th ACM SIGKDD Conference on Knowledge Discovery and Data Mining*, KDD ’22, page 936–944.
- Li, Y., Chai, S., Wang, G., Zhang, X., and Qiu, J. (2022c). Quantifying the uncertainty in long-term traffic prediction based on pi-convlstm network. *IEEE Transactions on Intelligent Transportation Systems*, 23(11):20429–20441.
- Li, Y., Yu, R., Shahabi, C., and Liu, Y. (2017). Diffusion convolutional recurrent neural network: Data-driven traffic forecasting. *arXiv preprint arXiv:1707.01926*.
- Lin, L., Handley, J. C., Gu, Y., Zhu, L., Wen, X., and Sadek, A. W. (2018). Quantifying uncertainty in short-term traffic prediction and its application to optimal staffing plan development. *Transportation Research Part C: Emerging Technologies*, 92:323–348.
- Lin, L., Wang, Q., and Sadek, A. W. (2015). A novel variable selection method based on frequent pattern tree for real-time traffic accident risk prediction. *Transportation Research Part C: Emerging Technologies*, 55:444–459.
- Lin, Y. T., Neumann, J., Miller, E. F., Posner, R. G., Mallela, A., Safta, C., Ray, J., Thakur, G., Chinthavali, S., and Hlavacek, W. S. (2021). Daily forecasting of regional epidemics of coronavirus disease with bayesian uncertainty quantification, united states. *Emerging infectious diseases*, 27(3):767.
- Liu, G., Jin, H., Li, J., Hu, X., and Li, J. (2022). A bayesian deep learning method for freeway incident detection with uncertainty quantification. *Accident Analysis & Prevention*, 176:106796.
- Liu, J. and Guan, W. (2004). A summary of traffic flow forecasting methods. *Journal of highway and transportation research and development*, 21(3):82–85.
- Liu, J., Li, T., Xie, P., Du, S., Teng, F., and Yang, X. (2020). Urban big data fusion based on deep learning: An overview. *Information Fusion*, 53:123–133.
- Liu, Z., Chen, Y., Xia, F., Bian, J., Zhu, B., Shen, G., and Kong, X. (2023). Tap: Traffic accident profiling via multi-task spatio-temporal graph representation learning. *ACM Transactions on Knowledge Discovery from Data*, 17(4):1–25.
- Lord, D. and Mannering, F. (2010). The statistical analysis of crash-frequency data: A review and assessment of methodological alternatives. *Transportation research part A: policy and practice*, 44(5):291–305.
- Lv, Y., Tang, S., and Zhao, H. (2009). Real-time highway traffic accident prediction based on the k-nearest neighbor method. In *2009 international conference on measuring technology and mechatronics automation*, volume 3, pages 547–550. IEEE.
- Ma, C., Zhao, Y., Dai, G., Xu, X., and Wong, S.-C. (2022). A novel stfsa-cnn-gru hybrid model for short-term traffic speed prediction. *IEEE Transactions on Intelligent Transportation Systems*.
- Ma, Z., Mei, G., and Cuomo, S. (2021). An analytic framework using deep learning for prediction of traffic accident injury severity based on contributing factors. *Accident Analysis & Prevention*, 160:106322.
- Mahmoud, N., Abdel-Aty, M., Cai, Q., and Yuan, J. (2021). Predicting cycle-level traffic movements at signalized intersections

- using machine learning models. *Transportation research part C: emerging technologies*, 124:102930.
- Mallick, H., Chatterjee, S., Chowdhury, S., Chatterjee, S., Rahnavard, A., and Hicks, S. C. (2022). Differential expression of single-cell rna-seq data using tweedie models. *Statistics in medicine*, 41(18):3492–3510.
- Moosavi, S., Samavatian, M. H., Parthasarathy, S., Teodorescu, R., and Ramnath, R. (2019). Accident risk prediction based on heterogeneous sparse data: New dataset and insights. In *Proceedings of the 27th ACM SIGSPATIAL International Conference on Advances in Geographic Information Systems*, pages 33–42.
- Pearce, T., Brintrup, A., Zaki, M., and Neely, A. (2018). High-quality prediction intervals for deep learning: A distribution-free, ensembled approach. In *International conference on machine learning*, pages 4075–4084. PMLR.
- Perozzi, B., Al-Rfou, R., and Skiena, S. (2014). Deepwalk: Online learning of social representations. In *Proceedings of the 20th ACM SIGKDD international conference on Knowledge discovery and data mining*, pages 701–710.
- Qian, W., Zhang, D., Zhao, Y., Zheng, K., and Yu, J. J. (2022). Uncertainty quantification for traffic forecasting: A unified approach. *arXiv preprint arXiv:2208.05875*.
- Ren, H., Song, Y., Wang, J., Hu, Y., and Lei, J. (2018). A deep learning approach to the citywide traffic accident risk prediction. In *2018 21st International Conference on Intelligent Transportation Systems (ITSC)*, pages 3346–3351. IEEE.
- Reza, S., Ferreira, M. C., Machado, J., and Tavares, J. M. R. (2022). A multi-head attention-based transformer model for traffic flow forecasting with a comparative analysis to recurrent neural networks. *Expert Systems with Applications*, 202:117275.
- Rodrigue, J.-P. (2020). *The geography of transport systems*, chapter 8 urban transport challenges. Routledge.
- Saha, D., Alluri, P., Dumbaugh, E., and Gan, A. (2020). Application of the poisson-tweedie distribution in analyzing crash frequency data. *Accident Analysis & Prevention*, 137:105456.
- Shi, P. (2016). Insurance ratemaking using a copula-based multivariate tweedie model. *Scandinavian Actuarial Journal*, 2016(3):198–215.
- Shirazi, M. and Lord, D. (2019). Characteristics-based heuristics to select a logical distribution between the poisson-gamma and the poisson-lognormal for crash data modelling. *Transportmetrica A: Transport Science*, 15(2):1791–1803.
- Smyth, G. K. and Jørgensen, B. (2002). Fitting tweedie’s compound poisson model to insurance claims data: dispersion modelling. *ASTIN Bulletin: The Journal of the IAA*, 32(1):143–157.
- Tang, J. and Zeng, J. (2022). Spatiotemporal gated graph attention network for urban traffic flow prediction based on license plate recognition data. *Computer-Aided Civil and Infrastructure Engineering*, 37(1):3–23.
- Thornton, P. E., Shrestha, R., Thornton, M., Kao, S.-C., Wei, Y., and Wilson, B. E. (2021). Gridded daily weather data for north america with comprehensive uncertainty quantification. *Scientific Data*, 8(1):190.
- Tobler, W. R. (1970). A computer movie simulating urban growth in the detroit region. *Economic geography*, 46(sup1):234–240.
- Trirat, P., Yoon, S., and Lee, J.-G. (2023). : Multi-view graph convolutional networks for traffic accident risk prediction. *IEEE Transactions on Intelligent Transportation Systems*.
- Tu, W., Zhu, T., Xia, J., Zhou, Y., Lai, Y., Jiang, J., and Li, Q. (2020). Portraying the spatial dynamics of urban vibrancy using multisource urban big data. *Computers, Environment and Urban Systems*, 80:101428.
- Tweedie, M. C. et al. (1984). An index which distinguishes between some important exponential families. In *Statistics: Applications and new directions: Proc. Indian statistical institute golden Jubilee International conference*, volume 579, pages 579–604.
- Veličković, P., Cucurull, G., Casanova, A., Romero, A., Lio, P., and Bengio, Y. (2017). Graph attention networks. *arXiv preprint arXiv:1710.10903*.
- Wang, B., Lin, Y., Guo, S., and Wan, H. (2021a). GSNet: Learning Spatial-Temporal Correlations from Geographical and Semantic Aspects for Traffic Accident Risk Forecasting. *Proceedings of the AAAI Conference on Artificial Intelligence*, 35(5):4402–4409.
- Wang, B., Zhang, C., Wong, Y. D., Hou, L., Zhang, M., and Xiang, Y. (2022a). Comparing resampling algorithms and classifiers for modeling traffic risk prediction. *International journal of environmental research and public health*, 19(20):13693.
- Wang, H. and Yeung, D.-Y. (2020). A survey on bayesian deep learning. *ACM computing surveys (csur)*, 53(5):1–37.
- Wang, K., Zhao, S., and Jackson, E. (2019). Functional forms of the negative binomial models in safety performance functions for rural two-lane intersections. *Accident Analysis & Prevention*, 124:193–201.
- Wang, Q., Wang, S., Zhuang, D., Koutsopoulos, H., and Zhao, J. (2023a). Uncertainty quantification of spatiotemporal travel demand with probabilistic graph neural networks. *arXiv preprint arXiv:2303.04040*.
- Wang, S. and Cao, J. (2021). Ai and deep learning for urban computing. *Urban Informatics*, pages 815–844.
- Wang, S., Chen, A., Wang, P., and Zhuge, C. (2023b). Predicting electric vehicle charging demand using a heterogeneous spatio-temporal graph convolutional network. *Transportation Research Part C: Emerging Technologies*, 153:104205.
- Wang, S., Zhang, J., Li, J., Miao, H., and Cao, J. (2021b). Traffic Accident Risk Prediction via Multi-View Multi-Task Spatio-Temporal Networks. *IEEE Transactions on Knowledge and Data Engineering*, pages 1–1.
- Wang, Y., Jing, C., Xu, S., and Guo, T. (2022b). Attention based spatiotemporal graph attention networks for traffic flow forecasting. *Information Sciences*, 607:869–883.
- Wang, Z., Jiang, R., Cai, Z., Fan, Z., Liu, X., Kim, K.-S., Song, X., and Shibasaki, R. (2021c). Spatio-temporal-categorical graph neural networks for fine-grained multi-incident co-prediction. In *Proceedings of the 30th ACM international conference on information & knowledge management*, pages 2060–2069.
- Wickelmaier, F. (2003). An introduction to mds. *Sound Quality Research Unit, Aalborg University, Denmark*, 46(5):1–26.
- Wu, D., Gao, L., Chinazzi, M., Xiong, X., Vespignani, A., Ma, Y.-A., and Yu, R. (2021). Quantifying uncertainty in deep

- spatiotemporal forecasting. In *Proceedings of the 27th ACM SIGKDD Conference on Knowledge Discovery & Data Mining*, pages 1841–1851.
- Wu, M., Jia, H., Luo, D., Luo, H., Zhao, F., and Li, G. (2022). A multi-attention dynamic graph convolution network with cost-sensitive learning approach to road-level and minute-level traffic accident prediction. *IET Intelligent Transport Systems*, page itr2.12254.
- Wu, Y. and James, J. (2021). A bayesian learning network for traffic speed forecasting with uncertainty quantification. In *2021 International Joint Conference on Neural Networks (IJCNN)*, pages 1–7. IEEE.
- Wu, Y., Ye, Y., Zeb, A., Yu, J. J., and Wang, Z. (2023). Adaptive modeling of uncertainties for traffic forecasting. *arXiv preprint arXiv:2303.09273*.
- Xue, J., Jiang, N., Liang, S., Pang, Q., Yabe, T., Ukkusuri, S. V., and Ma, J. (2022). Quantifying the spatial homogeneity of urban road networks via graph neural networks. *Nature Machine Intelligence*, 4(3):246–257.
- Yang, Z., Yang, Z., Smith, J., and Robert, B. A. P. (2021). Risk analysis of bicycle accidents: A bayesian approach. *Reliability Engineering & System Safety*, 209:107460.
- Yang, Z., Zhang, W., and Feng, J. (2022). Predicting multiple types of traffic accident severity with explanations: A multi-task deep learning framework. *Safety science*, 146:105522.
- Yu, B., Lee, Y., and Sohn, K. (2020a). Forecasting road traffic speeds by considering area-wide spatio-temporal dependencies based on a graph convolutional neural network (gcn). *Transportation research part C: emerging technologies*, 114:189–204.
- Yu, B., Yin, H., and Zhu, Z. (2018). Spatio-temporal graph convolutional networks: A deep learning framework for traffic forecasting.
- Yu, L., Du, B., Hu, X., Sun, L., Han, L., and Lv, W. (2021). Deep spatio-temporal graph convolutional network for traffic accident prediction. *Neurocomputing*, 423:135–147.
- Yu, R., Wang, Y., Zou, Z., and Wang, L. (2020b). Convolutional neural networks with refined loss functions for the real-time crash risk analysis. *Transportation research part C: emerging technologies*, 119:102740.
- Yuan, Z., Zhou, X., and Yang, T. (2018). Hetero-convlstm: A deep learning approach to traffic accident prediction on heterogeneous spatio-temporal data. In *Proceedings of the 24th ACM SIGKDD International Conference on Knowledge Discovery & Data Mining*, pages 984–992.
- Zhang, C., James, J., and Liu, Y. (2019a). Spatial-temporal graph attention networks: A deep learning approach for traffic forecasting. *IEEE Access*, 7:166246–166256.
- Zhang, C., Yan, X., Ma, L., and An, M. (2014). Crash prediction and risk evaluation based on traffic analysis zones. *Mathematical Problems in Engineering*, 2014.
- Zhang, Y. and Cheng, T. (2020). Graph deep learning model for network-based predictive hotspot mapping of sparse spatio-temporal events. *Computers, Environment and Urban Systems*, 79:101403.
- Zhang, Y., Cheng, T., and Ren, Y. (2019b). A graph deep learning method for short-term traffic forecasting on large road networks. *Computer-Aided Civil and Infrastructure Engineering*, 34(10):877–896.
- Zhao, L., Song, Y., Zhang, C., Liu, Y., Wang, P., Lin, T., Deng, M., and Li, H. (2019). T-gcn: A temporal graph convolutional network for traffic prediction. *IEEE transactions on intelligent transportation systems*, 21(9):3848–3858.
- Zhou, H., Qian, W., and Yang, Y. (2022a). Tweedie gradient boosting for extremely unbalanced zero-inflated data. *Communications in Statistics-Simulation and Computation*, 51(9):5507–5529.
- Zhou, Z., Wang, Y., Xie, X., Chen, L., and Liu, H. (2020). Riskoracle: a minute-level citywide traffic accident forecasting framework. In *Proceedings of the AAAI conference on artificial intelligence*, volume 34, pages 1258–1265.
- Zhou, Z., Wang, Y., Xie, X., Chen, L., and Zhu, C. (2022b). Foresee Urban Sparse Traffic Accidents: A Spatiotemporal Multi-Granularity Perspective. *IEEE Transactions on Knowledge and Data Engineering*, 34(8):3786–3799.
- Zhou, Z., Wang, Y., Xie, X., Qiao, L., and Li, Y. (2021). Stuanet: Understanding uncertainty in spatiotemporal collective human mobility. In *Proceedings of the Web Conference 2021*, pages 1868–1879.
- Zhu, L., Li, T., and Du, S. (2019). Ta-stan: A deep spatial-temporal attention learning framework for regional traffic accident risk prediction. In *2019 international joint conference on neural networks (IJCNN)*, pages 1–8. IEEE.
- Zhu, Y., Ye, Y., Liu, Y., and James, J. (2022). Cross-area travel time uncertainty estimation from trajectory data: a federated learning approach. *IEEE Transactions on Intelligent Transportation Systems*, 23(12):24966–24978.
- Zhuang, D., Wang, S., Koutsopoulos, H., and Zhao, J. (2022). Uncertainty quantification of sparse travel demand prediction with spatial-temporal graph neural networks. In *Proceedings of the 28th ACM SIGKDD Conference on Knowledge Discovery and Data Mining*, pages 4639–4647.

Appendix A. Tweedie Table

where μ, σ is the mean and the standard values of Gaussian Distribution.

Tweedie EDMs	ρ	$\kappa(\theta)$	ϕ	θ	$a(y, \phi)$
Normal	0	$\frac{\theta^2}{2}$	σ^2	μ	$\exp(-y^2)/2\sigma^2 - \log 2\pi/2)$
Poisson	1	$\exp(\theta)$	1	$\log \mu$	$1/y!$
Poisson-Gamma	(1,2)	$\frac{(\theta-\rho\theta)^{\frac{2-\rho}{1-\rho}}}{2-\rho}$	ϕ	$\frac{\mu^{1-\rho}}{1-\rho}$	Eq.5
Gamma	2	$-\log(-\theta)$	ϕ	$-1/\mu$	$\frac{\phi^{-1/\phi} y^{1/\phi-1}}{\Gamma(1/\phi)}$